Technical Report ISTC/MCE/SV/385

ISTC

ISRO-IISc Space Technology Cell
Indian Institute of Science
Bangalore

Hydrogen gas sensor on flexible substrates

(Final Technical Report)

S. Venugopal, EE, IISc
K. Nandakumar, LPSC, ISRO
S. Ingersol, LPSC, ISRO

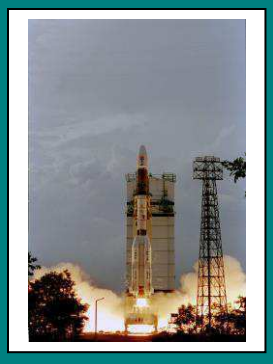

April 2019

ISRO-IISc Space Technology Cell
Indian Institute of Science
Bangalore

Hydrogen gas sensor on flexible substrates

(Final Technical Report)

S. Venugopal, ChE, IISc
K. Nandakumar, LPSC, ISRO
S. Ingersol, LPSC, ISRO

April 2019

Project Title: **Hydrogen gas sensor on flexible substrates**	Project Code: **ISTC/MCE/VS/385** Date of Commencement: **01/04/2017** Date of Closure **31/03/2019**
Investigator from IISc **Dr Venugopal Santhanam** Affiliation with email **Department of Chemical Engg, IISc** **svgpal@iisc.ac.in**	
Investigator from ISRO **Dr K Nandakumar (superannuated in 2018) and Mr S. Ingersol** Affiliation **LPSC**	
Type of the project: (Research/Development/etc.) **Development**	
Security classification if any: Open/Restricted **Open**	
Short Abstract (Maximum of 50 words) **Processes for fabricating palladium coated silver nanostructures on flexible substrates were developed. The devices showed a drop in resistance when exposed to hydrogen, attributed to the closing of nanoscale gaps due to the expansion of the palladium layer. In the best case, a response time of 38 seconds was recorded.**	
Keywords Flexible Leak Detector, Hydrogen, Printed Nanostructures, Palladium coated Silver, Resistive Sensors	

Total Budget (in lakh `) **14.88 Lakhs**
Products/methodology/algorithms delivered to ISRO/DOS Centre **Palladium nanostructure-based hydrogen gas sensor on a plastic substrate.** **Low-cost process for fabricating palladium coated conductive films onflexible substrates**
Where it is put into use/embedded in ISRO/DOS activities/programmes **The developed process can form the basis for developing low-cost hydrogen safety sensors and leak detectors in hydrogen handling facilities**
Number of JRF/students involved (give details of students PhD/MTech) **Project Assistants – 2** **Research scholars – 1, M Tech (Research)**
Number of papers published (International & National Journals/ Conferences etc) **1 - P. Joshi and V. Santhanam, "Strain-sensitive inkjet-printed nanoparticle films on flexible substrates", IEEE Sensors Letters, 2 (1), pp.1-4 March (2018)** (This was an offshoot of the process development efforts aimed at using plastic substrates for hydrogen sensing)
Patents **-NA-**
Details of visit(s) to ISRO centre(s). Include centre name, dates, host, nature of interactions (discussions/seminars) **LPSC- Bangalore, December 2018, Mr. S Ingersol, Discussions**

ACKNOWLEDGEMENTS

We would like to thank Dr K. Nandakumar for suggesting the topic of hydrogen gas detection/sensing and enlightening us on the magnitude of the issue. He had abundant time for discussions. His encouragement and professional approach made it a pleasure to interact with him.

We would like to thank Mr S. Ingersol for his crucial inputs regarding the nature of the substrate to be used and insightful discussions on the mode of sensing and detection.

Finally, We want to thank ISRO for funding and the STC staff for professional handling of the project implementation.

ABHISHEK RANADE

S. VENUGOPAL

ABSTRACT

The importance of hydrogen as a fuel is going to increase in the future as it has a high calorific value and causes no pollution upon conversion to water. However, properties such as its flammability, colourlessness, odourlessness and its tendency to leak through the smallest of gaps, even between atoms, make its use a dangerous venture. Such leaks can lead to the creation of explosive atmospheres, and if they are to be kept at bay, then it is essential to have a fast and reliable detection system so that appropriate action is initiated.

ISRO deals with liquid hydrogen carrying pipelines that stretch over several hundreds of meters. There is always the possibility of hydrogen leaking through the pipes, joints, bends or flanges. An economical detection system that can be wrapped around such probable areas of hydrogen leakage and which can respond to leakages in around a second is needed. Presently available technologies are not suitable for this type of application. The available detection systems can be broadly divided into two parts: (i) the detecting element- it is the active part of the detection system that is sensitive towards hydrogen and (ii) the transducer- which converts the sensor-hydrogen interaction into a signal, preferably electrical. Detection systems available in the market are based on various sensing materials that can transduce hydrogen concentration to an electrical signal. Palladium is the most commonly studied material in this aspect. When hydrogen is present around palladium, the hydrogen is absorbed into palladium and then forms palladium hydride. Palladium hydride has a lower bulk density and higher electrical resistance than palladium which leads to changes in volume and electrical properties after hydrogen absorption. These changes can be detected if the palladium-based detecting element is a part of an electrical circuit. The response time can be further reduced if nanostructures are used in the detecting element as they have a higher surface to volume ratio.

In this project, silver nanostructures were formed on a flexible substrate, such as paper, by the ‘print – expose – develop’ method. Palladium was coated on silver using a modified toning recipe. Furthermore, this process was adapted to Polyethylene terephthalate (PET) based overhead transparency (OHP) sheets, by using surface

roughening to enhance wettability. Both a flow-through testing setup and a diffusion chamber set-up were fabricated in accordance with the ISO 26142 guidelines for testing hydrogen sensors. The palladium coated silver nanostructure-based detecting elements showed a drop-in resistance when exposed to hydrogen, which is attributed to the closing of nanoscale gaps due to the expansion of the palladium films caused by the absorption of hydrogen. Films with higher palladium content were found to be more sensitive to the presence of hydrogen. In the best case, a response time of 38 seconds was recorded after exposure to 10.7% of hydrogen.

TABLE OF CONTENTS

LIST OF FIGURES

LIST OF TABLES

CHAPTER 1

INTRODUCTION

1.1 Need for hydrogen detection

Hydrogen (H_2) is emerging as a new source of energy to address the need for alternative renewable sources of energy amidst concerns of global warming [1]. There are various advantages of using hydrogen as the source of energy as it undergoes "clean" combustion, and as it is possible to be generated and recycled in a renewable fashion using water and solar energy. However, it is highly flammable with its lower explosive limit being 4% v/v in air [2]. Moreover, it is a colourless, odourless and tasteless gas, and so human senses cannot detect it. It is also the lightest element in the universe, which means its leakage risk, is high. It might seem that adding some odorant (e.g. ethyl mercaptan used in cooking gas) will solve this problem. However, odorants are not suitable in case of smelling hydrogen leaks as they are not light enough to 'travel with' hydrogen or to disperse at the same dispersion rate. Furthermore, odorants can also pollute the catalyst of fuel cells, which are very important to the hydrogen economy [3]. That is why using odorants for detecting hydrogen leaks is a whole new challenge. Also, in case of long pipelines carrying hydrogen, adding odorant will not make any sense. Hence it is imperative to have a system for fast and reliable detection of hydrogen gas in all the areas dealing with hydrogen.

The history of detecting and monitoring concentration of hydrogen dates back over 100 years, at filling stations for airships [4]. Presently, hydrogen sensing is necessary for areas like ammonia and methanol production, the hydration of hydrocarbons, the desulphurization of petroleum products and the production of rocket fuels. [5]. Fuel cells can directly convert hydrogen into electricity by combining it with oxygen to produce only water and no other harmful emissions. In the future hydrogen can be used to fuel vehicles, aircraft and provide power for our homes and offices [6].

1.2 Need for low-cost, flexible hydrogen detection

Conventionally, hydrogen is detected using gas chromatography or mass spectrometry in the laboratory, and by using handheld sensors in the field. Hydrogen sensors are devices that detect hydrogen gas molecules and produce a signal with a magnitude proportional to the hydrogen gas concentration [7]. When the H_2 molecules interact with the detecting element of a hydrogen sensor, some of its properties such as refractive index, temperature, mass, electrical resistance and some mechanical properties can get changed. These changes are then translated into an electrical signal, typically, by means of a transducer.

Different industries have set desirable timescales on which these changes ought to occur so that corrective action can be taken in case of a hydrogen leak. Doing so is essential as otherwise, a high enough hydrogen concentration build-up could end in disaster. The response time (t_{90}), which is the time taken to typically reach 90% of the final response to a change in hydrogen concentration [8], is a significant performance characteristic of hydrogen sensors/leak detection systems. Fuel cell car manufacturers desire a response time of less than a second as shown in Table 1.1 for hydrogen sensing platforms [9]. It also lists other desired performance characteristics values.

Table1.1: Desirable characteristics for hydrogen safety sensors. Reproduced from [9]

Parameter	Desired value
Measurement Range	0.1% - 10%
Operating Temperature	-30 to 80 °C
Response Time	< 1 s
Accuracy	5% of full scale
Gas environment	Ambient air, 10-98% relative humidity
Interference resistance	e.g. Hydrocarbons

ISRO Propulsion Complex (IPRC, formerly LPSC-Liquid Propulsion Systems Centre) division at Mahendragiri deals with liquid hydrogen carrying pipelines that stretch over several hundreds of meters. There is always the possibility of hydrogen leaking through the pipes, joints, bends or flanges. However, the handheld-instruments presently available are either unwieldy for monitoring corners in pipelines or slow in terms of response time to hydrogen or cannot be used online. So, there is a need for an economical detection system that can be wrapped around such probable areas of hydrogen leakage and which can respond to leaks in around a second.

1.3 Scope of the project

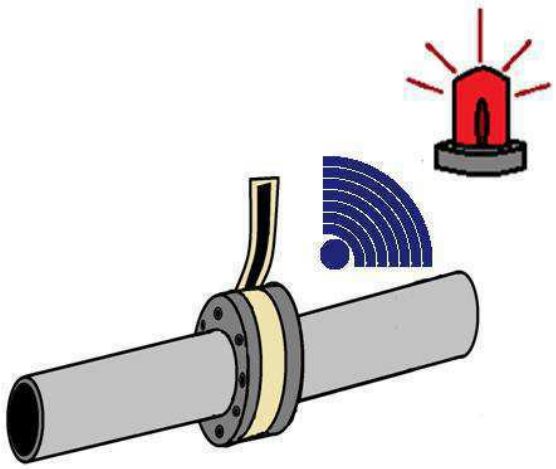

Figure 1.1: Schematic illustration of a flexible-substrate based hydrogen leak detection element wrapped around a flange for remotely monitoring hydrogen leaks.

The goal of this project is the development of a low-cost, flexible hydrogen detection tape for wrapping around liquid hydrogen carrying pipelines and flanges (Figure 1.1). IPRC at Mahendragiri handles liquid hydrogen storage tanks and transportation pipelines spread over a large area. Detecting hydrogen leakages at various locations is essential to ensure the safety of personnel and property. By wrapping/placing a non-flammable and flexible sensor/detector around such places, it will be possible to detect leaks in a remote manner.

In terms of contemporary technology being used, NASA employs a chemochromic tape, made by a mixture of PdO and TiO_2, that changes colour upon exposure to hydrogen. If pure hydrogen leaks, such a tape will change colour in a matter of about

10 s. If it is exposed to 1% H_2, then it has a response time of 3 min [10]. As such, there is ample scope for the development of an indigenous low-cost sensor/detector 'tape' that can respond to 1% H_2 in roughly a second. Non-flammability, rapid response, and insensitivity to contaminants such as CO, CH_4, SO_2 etc. are the other desired performance characteristics.

An earlier investigation in our group used inkjet-printed percolating silver nanowire networks as substrates for palladium deposition using the process of Galvanic displacement [11]. This earlier study had identified a lack of reproducibility in terms of response to hydrogen exposure as the critical issue. Galvanic exchange is reported to be rather complicated and poorly controlled, resulting in the formation of 3D palladium islands instead of a uniform overlayer [12]. Hence there was a need to avoid galvanic displacement reaction and to deposit palladium on silver in a uniform layered manner, such that repeatability can be ensured. Another observation of the earlier study was the incompatibility of the paper-based substrates with the gas sensing test platform used. With these issues in mind, the scope of this project was

1) To fabricate silver@palladium nanostructures on plastic substrates

2) To evaluate the response characteristics and selectivity as a function of different morphologies and nanostructure composition.

To achieve these aims, the strategy involved

1) developing a reliable process for uniform coating of nanoscale palladium overlayers onto conductive silver nanostructures, and

2) fabricating a hydrogen sensor testing setup as per ISO specifications.

CHAPTER 2

LITERATURE REVIEW

There are various technologies that are employed for the detection of hydrogen. They use different effects observed upon exposure of a certain material to hydrogen, palladium being the foremost against them.

2.1 Metal-oxide based resistive hydrogen sensor

Metal oxide sensors are commonly used [13] due to the low cost of fabrication, broad gas detection capability [8] and reasonable response times (< 20 s) [14]. Metal oxides, such as tin oxide (SnO_2), undergo changes in their electrical properties when they are exposed to reducing gases. Such sensors use a metal oxide film coated on an insulating substrate material that is electrically contacted by two electrodes (Fig 2.1) [5]. Typically, the oxide film is deposited on the substrate by means of screen printing followed by heat treatment to sinter it. Vapour deposition is another method used to deposit thinner films. The sensitive layer consists of an additive layer like Pd or Pt that improves the sensitivity of the oxide. A membrane is used to screen gases such as methane to avoid cross selectivity.

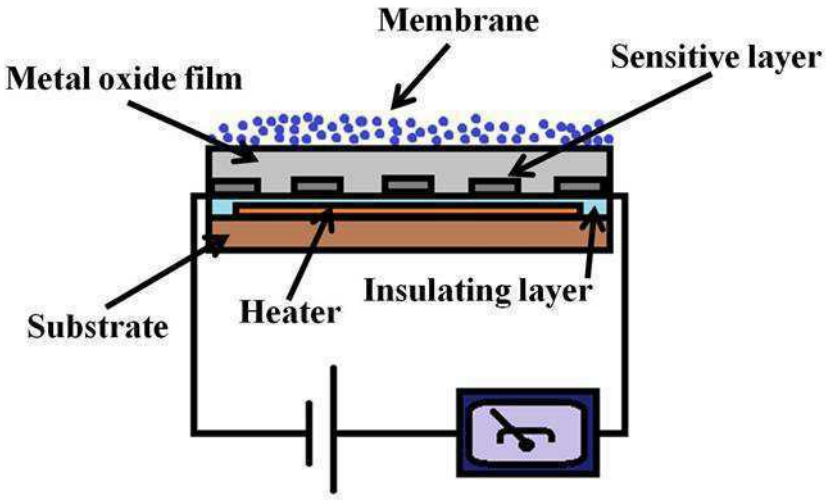

Figure 2.1: Schematic of metal-oxide based gas sensors. Reproduced from [5]

When in operation, this film is heated to a high temperature, which can be anywhere ranging from 180 °C to 450 °C depending upon the metal oxide film that is being

used. This heating is necessary to promote the reaction with the reducing gas and remove water formed in the reaction thereafter. The measured resistance of the detecting element changes as this reaction happens, which ultimately depends upon the concentration of the reducing gas available in the surrounding environment. A reasonable approximation of this dependence of resistance of the sensor element on the concentration of H_2 or any other reducing gas is given by:

$$R(c) = a*c*b$$

Here, c is the concentration of the reducing gas, and a and b are sensor specific constants.

The resistance change is calibrated in terms of the concentration of this gas, which is present in the environment. A sensor that is commonly available in the market that uses this technology is an MQ-8 hydrogen sensor.

Figure 2.2: MQ 8 hydrogen sensor module. Reproduced from [15]

It uses tin oxide (SnO_2) as the gas-sensitive metal-oxide layer. Reportedly, the reaction involved therein happens in two steps [5]. The first involves adsorption of oxygen on its surface, which decreases its surface conductivity. Then in the second step, hydrogen, if any, reacts with the adsorbed oxygen and the product is water vapour due to heating of the metal oxide film.

$$O_2 + 2\,e^- \longrightarrow 2\,O^-_{ads}$$

$$H_2 + 2\,O^-_{ads} \longrightarrow H_2O + e^-$$

The reduction of hydrogen releases electrons into the conduction band of the tin oxide that makes it an n-type semiconductor with increased conductivity. The concomitantly decreased resistance is then correlated in terms of hydrogen concentration.

Disadvantages of these types of sensors are that they are cross-selective to other gases such as CO, CH_4, alcohols etc. They consume more power owing to the high operating temperature required [13]. They also require the presence of oxygen for their functioning.

2.2 Combustible gas sensor

Hydrogen has a standard heat of combustion of 141.9 kJ/g, making its combustion a highly exothermic reaction. If such a reaction is carried out on the surface of a suitable catalyst, then the heat liberated can be used to detect the presence of hydrogen in the environment. The combustible gas sensors target this property for hydrogen sensing. For instance, a pellistor (pellet + resistor) type hydrogen sensor uses two platinum coils embedded in a ceramic bead or "pellet" (usually Al_2O_3) [5].

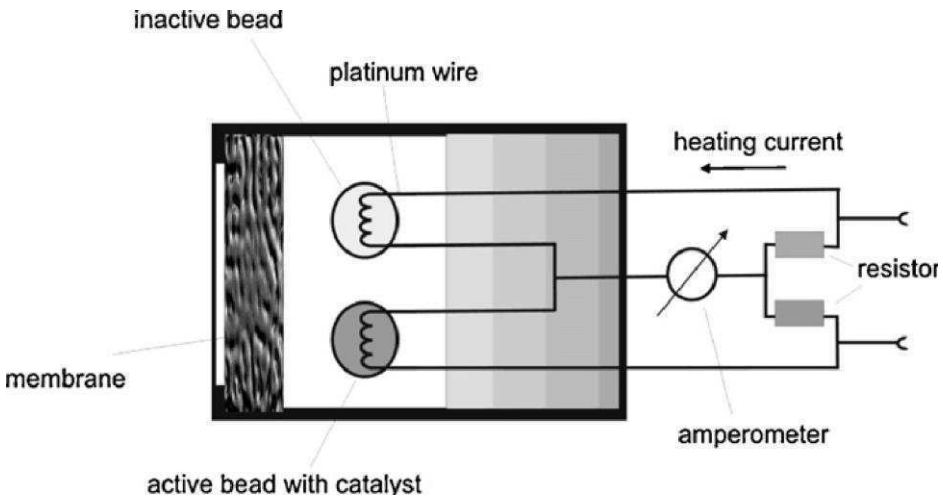

Figure 2.3: Schematic of a combustible gas sensor. The active and inactive pellets form a part of a Wheatstone bridge, the imbalance in which is used to sense hydrogen. Reproduced from [5]

The metallic coils work as heaters as well as being resistance thermometers. However, the surface of only one of those beads is activated with a noble metal like platinum or palladium. The other pellet has no catalyst. Both the beads are a part of a Wheatstone bridge circuit. During operation, electric current is passed through both the coils which cause them to heat up to nearly 300°C. In this condition, hydrogen molecules are chemisorbed on the catalyst and become oxidized (in the presence of oxygen), to

form water. This is an exothermic reaction that leads to the liberation of heat. The heat causes a change in electrical resistance of the activated coil. It leads to a disturbance in the Wheatstone bridge circuit which constitutes the sensor signal. This is a well-developed technology, and these types of sensors are widely available. They work until hydrogen concentrations of 4%. They need to be calibrated from time to time to account for their drift. However, their disadvantages are that they are also cross selective to other combustible gases such as hydrocarbons and carbon monoxide. The catalysts are also susceptible to poisoning from inhibitors.

2.3 Thermo conductivity sensors

These sensors utilize the difference in thermal conductivity between a reference environment and that of the gases to be measured. Thermal conductivity detectors measure the concentration of a gas in a binary gas mixture by comparing it to the thermal conductivity of a selected reference gas [8].

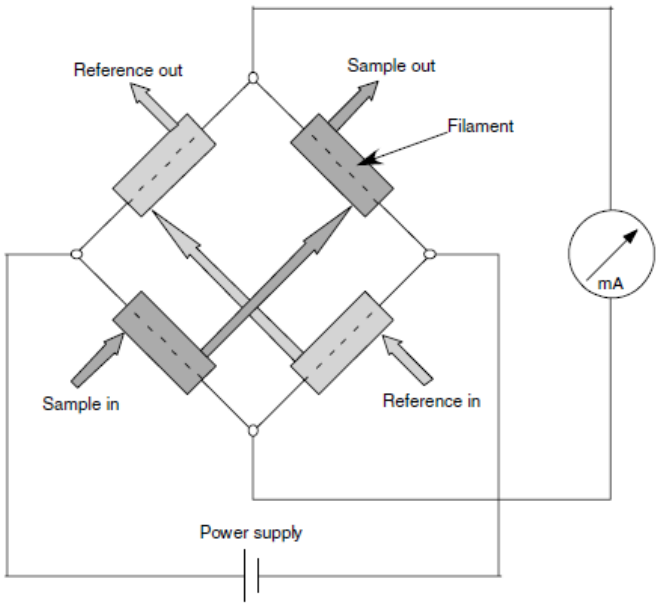

Figure 2.4: Schematic of a thermal conductivity-based gas sensor. Reproduced from [8]

In this sensor (Fig. 2.4), there are four ultrastable, precision glass coated thermistors. One pair is in contact with the sample gas and the other in contact with the reference

gas (like chlorine in a sealed chamber). The thermistors are mounted so that they are in close contact to the walls of the gas chambers. The whole cell is temperature controlled, and the thermistors are heated to an elevated temperature in a constant current Wheatstone bridge, like the pellets, are used in the combustible gas sensor. The thermistors lose heat to the walls of the gas chambers at a rate that is proportional to the thermal conductivity of the gas surrounding them. Hence each thermistor will have a different equilibrium temperature. The sensor will detect any gas that will alter the thermal conductivity of the gas chamber. In this way, a disturbance will creep into the Wheatstone bridge, which will then cause the sensor to give a signal.

2.4 Metal-based Resistive sensors

Like metal-oxide based sensors, this category of sensors employs pure metals or their alloys for detecting/sensing hydrogen. Palladium is most noted for its ability to selectively absorb hydrogen at ambient conditions, resulting in a change of electrical properties, refractive index, volume etc. On exposure of palladium to hydrogen, its resistance typically increases, due to the formation of palladium hydride. For a given set of conditions, palladium hydride has a higher electrical resistance than pure palladium.

All the technologies discussed so far have some strong points along with some shortcomings. These have been listed in Table 2.1

Table 2.1: Advantages and disadvantages of common hydrogen detection technologies. Reproduced from [16]

Hydrogen detection technologies	**Transduction mechanism**	**Advantages**	**Disadvantages**	**Application**
Combustible gas	Catalytic combustion (ΔR induced by ΔT)	Robust	Cross-sensitivity	Industry standard; Petroleum industry, infrastructure
Thermo-conductivity	Heat transfer (ΔR induced by ΔT)	Fast response time	Non-selective	Modelling studies; vehicles
Metal oxide	(ΔR) semiconductor doping	Low cost versatile	Reputation for instability, requires heating	Containers
Palladium thin film	Selective H_2 absorption	Selectivity	Prone to poisoning	Petroleum industry; specialized applications

2.5 Chemochromic Leak Detectors

The issue with the above-mentioned types of sensors is that as far as leak detection (which is the focus of this work) is concerned, they cannot reliably and accurately home in on the exact location of the leak. It is for this purpose that a different type of

hydrogen leak detector was developed for NASA, to be used at Kennedy Space Center (KSC) launch pad [17].

Figure 2.5: Chemochromic hydrogen leak detector tape wrapped around a flange of a pipe carrying H_2 at KSC, Florida. The colour of the tape changes from beige to dark grey upon exposure to H_2. Reproduced from [10]

It is a chemochromic detector that can change colour upon being exposed to hydrogen. It is flexible, unlike the above said solid state detectors, and hence can be wrapped around probable areas of leakage. In case of a leak, it changes colour, indicating that the leak has occurred very near to it. This enables to accurately home in on the leak. The detecting element is based on a mixture of PdO and TiO_2 which is the pigment as well as a protective coating. It is incorporated into a base polymer matrix. Such types of detectors can be made into any polymer part such as injection moulded plastic parts; fibre spun textiles or extruded tapes.

The resulting detector tapes were found to be irreversible in terms of their colour change, once exposed to hydrogen. They are found to be inexpensive, portable, and require no external power source for operation since they are devoid of any electronics. The colour change is noted by on the site inspection. That constitutes one disadvantage of these types of tapes, in that they can only be checked for leaks after the process has stopped. However, they are the most suitable technology compared to other contemporary ones discussed earlier as far as leak detection along pipelines is concerned.

This analysis of the literature reports suggests that a new type of detector is needed, different from the solid-state detectors commonly used, for accurately and reliably

locating leaks. The advantages of using palladium, compared to other materials used like metal oxides, for instance, are its selectivity for H_2, fast response time, operation at room temperature and low power consumption. Such palladium-based sensors can easily achieve the sensor requirements, at the same time not being affected by other gases and have been studied widely. Furthermore, the electrical resistance-based hydrogen detection has several advantages compared to other technologies such as overall performance level, the simplicity of detector structures, miniaturization, manufacturability and compatibility of sensor fabrication process with existing manufacturing process [18].

2.6 Response mechanisms of palladium-based sensors

Two modes of response mechanisms have been identified for palladium-based sensing of H_2 [19]: 1) Typically, in continuous palladium-film based sensors, the hydrogen molecule dissociates into atoms upon adsorption. These hydrogen atoms are then absorbed into the palladium lattice to form hydrides, which serve as scattering centres for electron transport. This scattering, in turn, increases the resistance of the palladium detecting element. In this mechanism, the measured resistance increases with an increase in the H_2 concentration (Fig. 2.6).

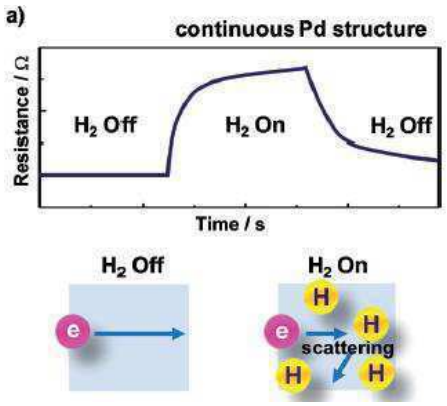

Figure 2.6: Schematic illustration of the increasing resistance mechanism for hydrogen sensing. Reproduced from [19]

2) In nanostructured palladium thin film sensors, the structures have 'nanoscale-gaps' between them, and upon exposure to hydrogen and its subsequent absorption, there is a 3.5% volume expansion due to the influx of H atoms into the palladium lattice. This expansion causes the nanoscale-gaps to close, thereby making possible the flow of current, just like a switch in ON state. Thus, on exposure to H_2, these types of sensors show a decrease in resistance (Fig. 2.7). Sensors undergoing such a mechanism upon exposure to H_2 have a faster response than the ones undergoing an increase in resistance, as the additional step of phase change of absorbed hydrogen into palladium hydride is not required in the case of nanoscale-gap based hydrogen sensors.

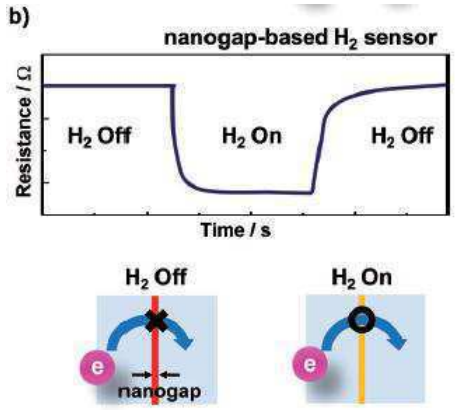

Figure 2.7: Schematic illustrating nanoscale-gap closing mechanism for hydrogen sensing. Reproduced from [19]

2.7 Silver-palladium alloy-based materials for hydrogen detection

Nanostructured palladium thin films facilitate hydrogen adsorption as well as desorption, thereby finding use in areas which are prone to hydrogen leakages frequently. However, pure Pd when exposed to H_2 undergoes volume expansion due to the higher lattice constant of palladium hydride. This repeated volume expansion and contraction of Pd can lead to embrittlement of pure Pd film-based hydrogen sensors over time, even for 100 nm thick palladium films on cyclic exposure to 2% H_2 (Fig. 2.8). Thus, the usage of pure Pd in the form of films places the reliability and accuracy of such sensors at risk due to the occurrence of such irreversible structural deformations [18]. One of the solutions is to use the alloys of Pd such as Pd-Mg, Pd-Au, Pd-Ag and Pd-Ni. Among these, the Pd-Ag system and its interaction with hydrogen

have been studied extensively. It has a high hydrogen selectivity as well as permeability higher than pure Pd, even at low H_2 pressures of several tens of torr. Studies using a kinetic simulator revealed that Pd-Ag alloy has a lower H_2 absorption capacity than pure Pd, which implies that this alloy is expected to have a faster response time and a lower H_2 detection limit. The alloying will also help overcome the problem of hydrogen embrittlement seen in pure Pd. All these properties make Pd-Ag an attractive choice for use as a detecting element [20].

When pure palladium and its gold, platinum and silver alloy membranes (25 µm thick) were tested at 350 °C and 300 psig [21], it was found that the Pd-Ag alloy shows remarkably high permeability towards H_2, almost 1.73 times that of pure Pd, higher than any other Pd alloy, at an optimum Ag loading of 23 wt%. Also, this Pd-Ag alloy was dimensionally stable and was not damaged upon H_2 cycling [22].

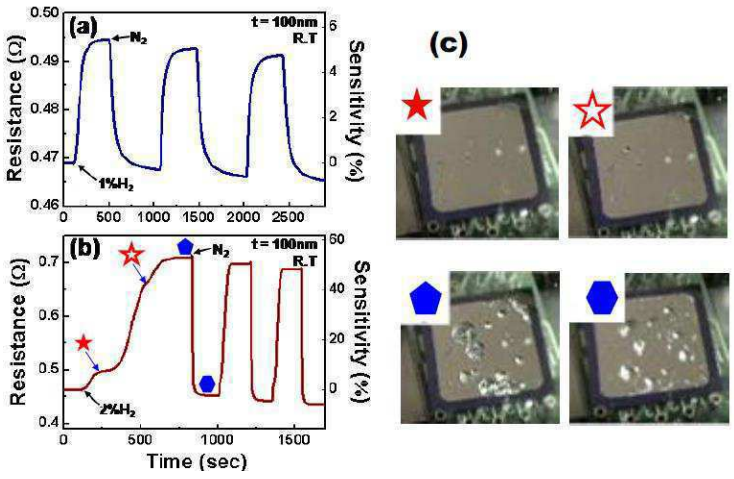

Figure 2.8: Electrical resistances and the corresponding sensitivities of a 100 nm-thick Pd thin film in response to (a) 1% H_2 and (b) 2% H_2 at room temperature. (c) Film morphologies at the steps indicated by the respective symbols in (b). Reproduced from [18].

From the perspective of low-cost fabrication, it is easy to fabricate silver nanostructures on flexible substrates. The halide salts of silver are sensitive to light; hence nanostructures can be made from silver using the print-expose-develop process. Thermodynamically also H_2 absorption is most favoured with the Pd-Ag system [23].

Ag-Pd bimetallic system is on par with pure palladium films at selectively absorbing H_2. However, recalling the requirements for a sensor with fast response time, it is also necessary to consider the kinetics of this process of hydrogen absorption. The first step in the formation of any metal hydride is the dissociation of H_2 into H atoms on the metal surface. Palladium can do it with minimal activation barrier at ambient conditions as compared to other metals that need increased hydrogen pressures or temperature [24,25]. The mechanism for H_2 absorption is schematically shown in fig 2.9 [26]. Upon exposure of palladium to H_2 (Fig 2.9(a), the gas molecules get adsorbed on the surface of palladium (Fig 2.9(b)) and thereafter get dissociated into individual atoms (Fig 2.9(c)) [27]. The hydrogen atoms continue moving by diffusion through high diffusivity tracks like grain boundaries, dislocations or even by vacancy exchange mechanism [28–31] and ultimately occupy an octahedral interstitial site in the Pd lattice (Fig 2.9(d)), which means the number density of defects in palladium lattice will decide its H_2 uptake capacity [18]. Thus, palladium gets converted into palladium hydride, with the H concentration ultimately determining whether it is in the α phase or β phase or a mixture of both. If the thickness of Pd film is above a certain 'critical' thickness, the bulk diffusion is the rate determining step, whereas in nanostructured films having a thickness less than the critical thickness, the hydrogen absorption rate of Pd is limited by other processes. Modelling studies [32] show that at temperatures above approximately 573 K for clean Pd, this critical thickness is about 1 μm. In the case of nanowire morphology, it has been found that the surface reactions such as H_2 adsorption and desorption are the rate-limiting step [33].

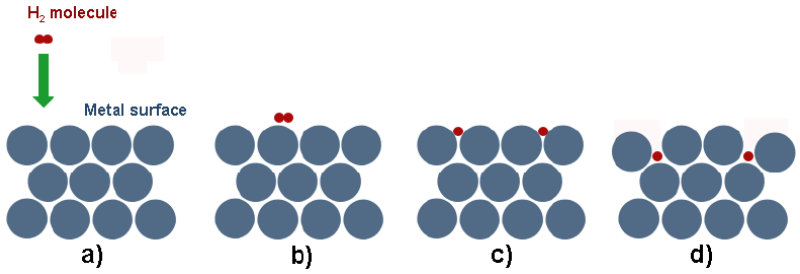

Figure 2.9: Schematic illustration of the mechanism of formation of metal hydrides by dissociative adsorption and diffusion. Reproduced from [26]

To summarize, it is desirable to fabricate a hydrogen sensor using Ag-Pd based detecting element in the nanoscale regime, so that:

1) H_2 diffusion in bulk Pd that causes its embrittlement can be avoided

2) Due to the larger surface area to volume ratio in the nanoscale regime, a faster response can be obtained as compared to bulk films.

CHAPTER 3

MATERIALS AND METHODS

This chapter describes the protocols used for fabricating and characterizing the hydrogen detecting elements.

3.1 Silver nanostructure formation using inkjet printing

Silver nanostructures were printed on drawing paper using a print-expose-develop methodology [11]. An inkjet printer available commercially, HP 1010, was used for printing aqueous solutions. HP 802, small black cartridges, were broken open and the ink was washed away completely using normal water. MS Powerpoint was used for generating patterns to print. The printer settings were kept as: "Photo paper with best quality" and "High-quality grayscale". The average volume per print was found by printing DI water and weighing the cartridge before and after printing, which came out to be ~1.2 μL/cm^2. For generating silver nanostructures. two separate cartridges are filled with 0.5 M $AgNO_3$ (99.9%, SD Fine Chemicals Ltd) and 1 M KX. Here KX is a mixture of KBr (>99%, SD Fine Chemicals Ltd) and KI (>99%, Merck) in 95:5 weight ratio. Both the solutions were sonicated in an ultrasonicator (Branson 2510E, 42 kHz) for 5 minutes, to dissolve the salts properly, which also helps in avoiding cartridge clogging. The solutions were printed alternately, starting from KX, three times (KX – $AgNO_3$ – KX – $AgNO_3$ – KX – $AgNO_3$). The cartridge is filled with roughly 120 μL of solution, as the area required to be printed was taken as 6 squares of 16 cm^2 area each, with cartridges printing 1.2 μL for every square cm. Exposure involved keeping these printed patterns at a distance of 50 cm below a halogen lamp for 15 min immediately after printing. D-76 developer was prepared and used for developing the exposed silver halide patterns. 1 L of this developer consists of 100 g sodium sulphite (97%, SD Fine Chemicals Ltd), 2 g metol (99%, SD Fine Chemicals Ltd), 5 g hydroquinone (99.5%, SD Fine Chemicals Ltd) and 2 g borax (98%, Fisher Scientific). The patterns were developed for 15 min. After developing, the patterns were washed in DI water for 10 minutes to rinse off the developer. These printed squares were stored in plastic covers and kept in the dark prior to future use.

The printed squares were cut in smaller pieces of 1 cm by 1 cm sizes to be used further for toning. These squares, once toned with Pd, are called as detecting elements in this report.

3.2 Pd toner preparation

The toner solution was prepared by adding 167.9 mg of citric acid monohydrate (99.5% SD Fine Chemicals Ltd) in 20 mL DI water followed by 14.1 mg of $PdCl_2$ (99.9%, Sigma Aldrich). The $PdCl_2$ takes a couple of hours to dissolve completely. This solution is referred to as "standard toner" or "normal toner" in this report.

To prepare coffee-added toner 15.9 mg of 'Bru Instant' was added per mL of normal toner, well-mixed and allowed to stand for 1 h. The coffee-added toner is then ready to use after this waiting period. Once toning is done with, the substrates are washed in DI water for 10 minutes to remove the excess toner.

3.3 Citric acid pre-treatment

Citric acid pre-treatment involves preparing a 20 mL solution having 328 mg of citric acid monohydrate in DI water. Then the silver nanostructure patterns are immersed, face first, into this solution. It is kept for 1 h in this way if paper-based Pd toning is to be done. Preliminary experiments showed that to obtain sufficient palladium deposition on OHP substrates citric acid pretreatment must be carried out for 18 h.

3.4 Method of resistance measurement:

A two-probe multimeter was used for obtaining the data in fig 4.9. The leads were placed 1 cm apart from each other, and the resistance was measured along any diagonal. For hydrogen sening measurements, a Keithley 6221 – 2182A current source – nanovoltmeter combination in a four terminal configuration was used to avoid disturbance due to contact resistances.

3.5 Material Characterization

FESEM imaging: All the samples of detecting elements were washed with DI water, dried and desiccated for 12 hours prior to FESEM imaging. All the samples have been

sputtered with gold with a sputtering time of 80 s and a sputtering current of 20 mA to facilitate EDX analysis. The samples were scanned in a few different areas, and the EDS elemental analyses have been averaged for at least 4 different regions in any given sample

Optical profilometry: Plastic OHP substrates were prepared by cleaning in acetone and then DI water. They were dried and sputtered with gold for 200 seconds at a sputtering current of 20 mA to form a reflective coating on the surface.

XPS: Samples for XPS were prepared by cutting small pieces of detecting elements, sticking them on a piece of carbon tape, which is then stuck on a larger piece of OHP.

UV-Vis spectrophotometry: The standard toner sample was prepared by first preparing the normal toner as mentioned previously. UV- vis spectrophotometry was performed on it by taking 200 µL of this solution in a quartz cuvette and then adding 2 mL of DI water to it. The UV-Vis spectrophotometry of the coffee toner solution was performed as below:

(i) 1 mL of the coffee toner was prepared by the method mentioned earlier. 9 mL of DI water was then added to it.

(ii) 10 µL of this solution was taken in the cuvette, and further 3 mL of DI water was added to it.

3.6 Detector testing setups

As per ISO 26142, hydrogen sensors can be tested for their performance viz. sensitivity, response time, recovery time etc. in two types of setups. This report emphasizes testing the detecting elements by both the methods mentioned in ISO 26142, as both offer distinct advantages.

3.6.1 Flow-through setup

Here, the response time of a sensor is characterized under dynamic conditions and is reliant on the convective transport of the test gas to the sensor's detecting element [34].

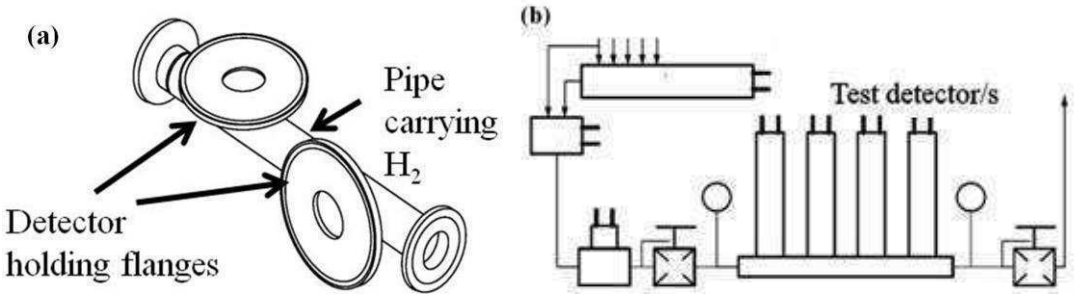

Figure 3.1: (a) The test manifold consists of a 25 mm ID pipe on which the flanges carrying the sensors/detectors are mounted, while gas passes through it (b) The entire flow through setup has temperature and humidity meters, test gas selectors, switches as per ISO standard [35]

The flow-through mode allows one to check the performance of the sensor in pipelines. There are various industries and power plants that have such scenarios. The hydrogen concentration in such pipes can vary from time to time, depending on the process concerned, and hence it becomes critical to monitor continuously so that the concentration does not exceed the specified limit. Thus, this method allows continuously varying the hydrogen concentration online and measuring the response. The diffusion chamber scenario, on the other hand, may be visualised as mimicking the scenario in pressurized hydrogen storage vessels, and wherein any leakage is desired to be detected as quickly as possible. This method is most preferred for measuring the response time of the detecting elements for most practical applications.

Figure 3.2 shows the as-fabricated flow-through setup. It consists of a 1" ID SS pipe with two T-joints, meant to house the detecting element. The T – joint holds a flange that has the detecting element, developed in the laboratory, placed between the upper and lower halves of the flange.

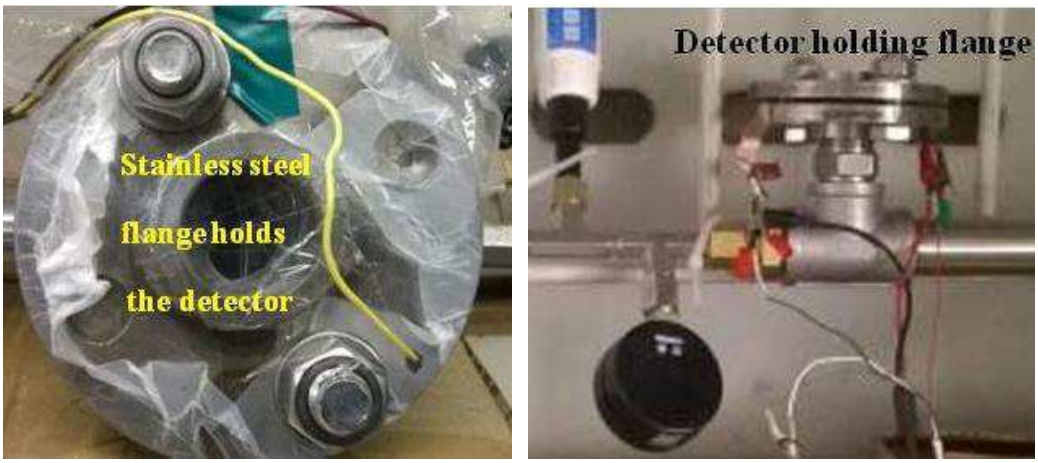

Figure 3.2: (Left) Detecting element in test manifold. (Right) Sensor housing flange

Figure 3.3: (Left) O-ring seal used in sensor holding flange. (Right) Keithley 6221-2182A used to measure sensor response

An O-ring kept in between both the flanges acts to keep the flowing gas from leaking out of the system. A piece of overhead transparency is used as a support for the detecting element so that it does not flutter when gas passes over it. Copper tapes extend out of the flanges and provide an electrical extension to the small (usually 1cm × 1cm) detecting element. The response from this detecting element is recorded by connecting it to a Keithley 6221 – 2182A current source – nanovoltmeter combination

in a four terminal configuration to avoid disturbance due to contact resistance. The Keithley 6221 current source can source a constant current ranging from 0.01 A down to nanoampere level. The 2182A nanovoltmeter can measure the resulting voltage changes that happen across the detecting element. Upon sourcing of current pulses by performing a pulsed delta test, the data can be read into a remote PC through an Ethernet cable. The resistance vs time plot can subsequently be plotted to get an estimate of the sensor response with time.

There are digital temperature and humidity meters installed at the beginning and end of the test section as is instructed by the ISO guidelines. Pressure gauges are also fixed at the inlet and exit likewise. An Athena Technology© ATH - 300 H_2 generator produces hydrogen by electrolysis of a 'caustic' KOH solution. Nitrogen from a cylinder is mixed with it in a T-junction before entering the test section. The flow rate of H_2 relative to that of N_2 can be used to determine the concentration of H_2 in the gas mixture. By ideal gas law, the flow rate is related directly to the molar flow rate.

It is vital to leak-proof the system as much as possible for two reasons mainly: (i) Loss of valuable H_2 and N_2 gas to the surroundings. (ii) The measured flow rates in the rotameter will be higher than the actual flow rate in the pipe leading to higher residence time which cannot be determined. Sources of leaks in the pipeline were found to be: (i) Temperature and humidity meter (× 2), ports of which were slightly larger than the probe diameter of the meters leading to gas leakage. For the first part, a rubber band stuffed in the gap between the meter probe and the inner wall of the meter port held the meter tightly in place. For sealing the gas flow leaking through this rubber band, a ziploc® bag with a hole that was just big enough to allow the meter's bolt to pass through was fitted along with the port in the pipe. The ziploc® bag was locked, during gas flow. Gas flow caused the bag to be filled first. When the pressure in the main pipe became equal to the pressure in the bag, no more gas would then flow in the bag, and convective flow occurs through the pipe after that, as long as there was at least one exit in the pipe. Sealing of the other meter was done in the same way.

Figure 3.4: Ziploc bag used to seal the temperature and humidity meter port

3.6.2 Diffusion chamber setup

This setup measures the response time of sensors under static conditions and relies on the diffusion of the test gas to the sensor's detecting element.

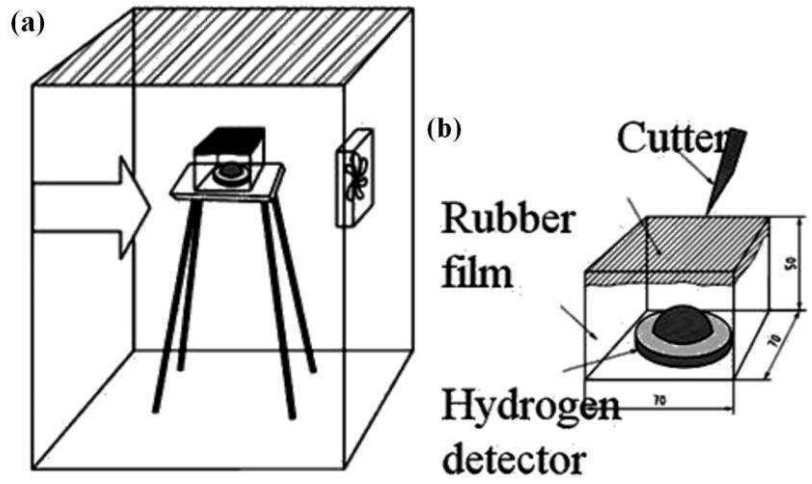

Figure 3.5: (a) The diffusion chamber setup consists of a box containing a circulatory fan facing the gas inlet (marked with arrow) and a sensor housing box which holds the sensor. (b) The sensor housing box holds the sensor which is sealed from the external using a rubber film which can be cut from outside the box [Reproduced from [35]]

To prepare this setup, acrylic sheets were used to make a box of dimensions 50 cm × 33 cm × 33 cm. Till the box attains desired H_2 concentration, H_2 gas continues to fill.

A smaller plastic box meant to be used as the sensor holding box is kept inside this box. A circulation fan having a flow rate capacity of at least 0.48 m^3/s is recommended to be used [36]. For this purpose, a Havells I-cool 180 mm fan is used which has a manufacturer specified flow rate of 0.66 m^3/s. Ports are made in the wall of the bigger box for wire connections. A temperature and humidity meter is kept inside the box for monitoring the conditions in there.

Figure 3.6: (Left) Diffusion chamber setup for sensor testing containing circulation fan and sensor holding box. (Right) Wires from Keithley 6221-2182A to measure the signal from the sensor

The smaller box has a hole at its top from where gases will flow directly onto the detecting element. The signal from here will be measured by the Keithley 6221 - 2182A system. The idea here is to try to emulate a sudden leak in the system. A heavy plate kept on a small piece of natural rubber and an O-ring is used to block the hole from the outside environment. As H_2 is flowing in the bigger box, the fan is kept on for homogenising the environment. After some time, when the required amount of H_2 has come into the box and become thoroughly homogenised, the fan is switched off. Then the heavy plate kept on top of the smaller box is slid off with the help of a lever from outside the box, so that the hole is suddenly exposed to the H_2 gas, thereby mimicking a leak.

3.7 Using the Keithley 6221-2182A equipment

The work done until now in this project involves preparation of the detecting elements only. The electronics involved therein are not developed till now. Hence there must be a way to connect the paper/plastic-based detecting elements to some

electronic equipment that can translate the changes occurring in this element to some electronic signal that can indicate presence or absence of hydrogen. The palladium involved in this detecting element upon exposure to hydrogen can respond in several ways such as a change in electrical resistance, optical properties like refractive index, size expansion etc. Out of these methods, the method to detect a change in electrical resistance was favoured as it is better suited for the purpose of detecting hydrogen leaks remotely from the pipelines at ISRO, Mahendragiri. It is also easier to fabricate compared with the other sensing technologies. Hence it was desired to measure the changes in electrical signals as the method to proceed for hydrogen sensing. The detecting elements developed undergo changes in electrical resistance upon exposure to hydrogen environment. In either mechanism of hydrogen sensing, i.e. resistance increase due to the formation of palladium hydride, or resistance reduction due to nano-gap closing, which can be measured accurately by supplying a constant current through the element and measuring the voltage fluctuations resulting thereon.

The Keithley 6221 is a current source that can maintain DC currents from as low as 0.1 pA to 105 mA. It has a high sourcing accuracy and built-in control functions which are best suited for resistance measurements in fields of nanotechnology for instance. It can be combined with 2182A nanovoltmeter, which can be treated as a single instrument that can not only supply constant current in a variety of tests but also record and store the corresponding voltage readings in synchronization with each other individually.

The reference manual for Keithley 6221 current source [37] was followed to set up the instrument tests. The two instruments were combined using an RS-232 cable and a Trigger link (8 pin DIN male to the male connector) cable. The power cables were also connected thereafter to the power outlet. A BNC to alligator clip connector cable was attached to the 6221, while a 2107 input cable was connected to the front of the 2182A nanovoltmeter as indicated in the manual [38]. Alligator clips were screwed at the end of the copper lugs of this cable to provide means of contact with the detecting element. The 6221 comes with a buffer which is memory storage, that can store the readings sent to it by the 2182A over the RS-232 cable. It can store up to a maximum of 65536 readings. There was a need to record data from the 6221 into a remote PC

because the readings had to be reported further. Hence an Ethernet cable was used to establish a connection with the laptop, in this case. There is a need to set the IP address, Subnet and the Gateway of the instrument whenever it is supposed to be used for remote operation with a PC. The method to do that is shown in Appendix A. The software that was used for this project are listed below:

1) Keithley configuration wizard

2) Keithley communicator

3) KI 6220 example software

All the software can be downloaded from the www.tek.com website.

The first one, i.e. the Keithley configuration wizard is used to establish new or edit existing configurations in terms of the instrument type, communications bus type, instrument addressing information, and communications settings. The second one is used to send commands from the PC to the combined 6221-2182A instrument when remote operation is being used. It also serves as a platform for getting the readings stored in the buffer. The third is not so much used in this project apart from getting readymade SCPI programs to feed to the instrument in the communicator. After setting up the instrument, a pulsed delta test was chosen as the desired test method for measuring voltage readings. The pulsed delta method passes pulses of current in the intervals of milliseconds to microseconds, to avoid Joule heating of the detecting element. The program that was used is provided in Appendix B.

The readings obtained thereafter are stored in the buffer, which can be obtained in the PC after the test is complete, through the communicator.

3.8 Test calculations

3.8.1 Test gas concentration

Test gas concentration in the flow through setup was found out by finding the volume fraction of H_2 in the test gas i.e.mixture of both H_2 and N_2. Since the gases are at ambient temperature and just above atmospheric pressure, it is safe to assume ideal gas law for both H_2 and N_2, since their first virial coefficients (Z_0) are ~1 (1.02 and 0.98, respectively). As a result, their volumes are additive. For instance, H_2 at 300

mL/min and N_2 at 4 L/min will give H_2 concentration (%) in the test gas as (0.3) * 100 / (0.3 + 4) = 6.98 %.

In the diffusion chamber setup, the test is performed in air. H_2 inlet flow rate is fixed at 300 mL/min. It is kept on for 3 minutes. Assuming the chamber is leak proof to H_2 over the duration of the test and H_2 being at atmospheric pressure, the H_2 concentration (%) is calculated as:

(Flow rate of H_2) * (Filling duration) *100 / [((Flow rate of H_2) * (Filling duration)) + (Volume of air in the box)]

Volume of air in the box is taken as the internal volume of the box, i.e. 33*33*50 cc = 54.45 L

Hence H_2 is kept on for 3 minutes at 300 ml/min, the concentration of H_2 (%) in the diffusion chamber for that particular test would be: 0.3*3*100/[(0.3*3) + 54.45] = 1.62%

3.8.2 Response time

The response time for any test, that has been used in this report is calculated as:

(i) finding the time required to reach 90% of the minimum value of the sensitivity signal from the stable baseline recorded in any given test, regardless whether that signal has saturated or not. The graph in Fig. 5.3 (h) saturates just before switching off hydrogen, after which it drops again. The response time for this has been calculated based on the first drop taken as the minimum value. Since the second drop is a feature of the test setup and not the detector, it has not been considered for response time calculations.

(ii) subtracting the time until which no H_2 has been introduced in the system, from (i),In case of diffusion chamber this is the time until which the lid on the housing hasn’t been removed.

CHAPTER 4

PALLADIUM DEPOSITION ON SILVER NANOSTRUCTURES

4.1 Palladium deposition using photographic toning recipe

The driving force for the Galvanic exchange reaction is the higher reduction potential of Pd^{2+} ions as compared to Ag^{+} ions, leading to the displacement of Ag^{+} ions into solution to form AgCl and subsequent formation of Pd^{0} clusters unevenly on top of silver nanowires. However, if the silver is protected by some molecule that can reduce its dissolution by palladium, or if the $PdCl_2$ solution is reduced beforehand so that all the Pd^{2+} is reduced to Pd^{0} and deposited on the silver nanowires, then it might render a more uniform coating of palladium on silver. In photography, toning refers to either replacement or coating of the outer layer of silver with another more noble metal, for both enhancing the longevity of the image and changing the tone (fig. 4.1 [39]) of the print. So, we used a standard palladium 'toning' solution, consisting of 3.98 mM of $PdCl_2$ and 80 mM of citric acid monohydrate. Citric acid has a moderate reducing power in that it enables reduction of palladium at room temperature, thus facilitating the process of toning. Also, since it has a strong interaction with metals, it can help reduce the dissolution of silver by galvanic displacement [12]. This recipe for the 'toning' solution is used in 'kallitype' printing, wherein the developed silver-based photographs are toned with different solutions such as platinum, gold, iron, palladium etc. [40].

Figure 4.1: Colour photograph (left) and its sepia toned version (right) Reproduced from [39]

Silver nanowires were obtained on paper as described earlier (see Section 3.1). After drying the paper, the silver part was cut into squares of 1 cm by 1 cm and dipped into the toner solution kept in plastic bottle caps, as shown in fig 4.2. The part which is under the clip is the printed part of the square, on which deposition is desired. No part of clip dips inside the toning solution.

Figure 4.2: Setup for holding 1x1 cm^2 substrates of silver nanowire on paper for Pd toning. The blue cup holds the toning solution while the clips hold the paper substrate

Figure 4.3 shows silvery flakes floating on the surface of the toner solution after 3 h. This suggests that galvanic displacement was not suppressed by this recipe. The toning duration was kept this long just for this sample, to unambiguously capture these silvery flakes, which indicate that the Pd deposition is galvanic in nature.

Figure 4.3: Silvery flakes are seen floating on top of the toning solution after 3 hours of dipping the substrate in a standard toner solution.

4.2 Addition of Instant Coffee Powder to Suppress Galvanic Displacement

To avoid galvanic displacement of silver by palladium, there is a need for reduction and stabilization of Pd^{2+} ions. Coffee powder contains caffeine/polyphenols that can

act as both reducing and capping agent to form palladium nanoparticles [41]. Caffeine polyphenols can also form complexes with metal ions in solution that can suppress galvanic displacement reaction. Based on preliminary experiments, 159.1 mg of Bru© instant coffee powder was added to 10 mL of the toner solution, mixed well, and allowed to stand for half an hour to form a palladium nanoparticle solution. The pH of the toning solution did not change significantly upon adding coffee powder to the solution and was estimated to be in the range of 2-3 based on the use of pH indicator papers. UV-visible spectroscopy shows that the absorption peak near 412 nm [42], attributed to the presence of Metal-Ligand Charge Transfer (MLCT) in palladium chlorohydride (formed by partial hydrolysis of palladium chloride) disappears after the addition of coffee (Fig.4.4). The disappearance indicates that either the Pd^{2+} has been reduced or that the chloride ions complexed with Pd^{2+} have been displaced after the addition of coffee powder. Gouda et al. [41] have shown TEM images confirming the presence of palladium nanoparticles 30 min after the addition of instant coffee powder to palladium chloride solution.

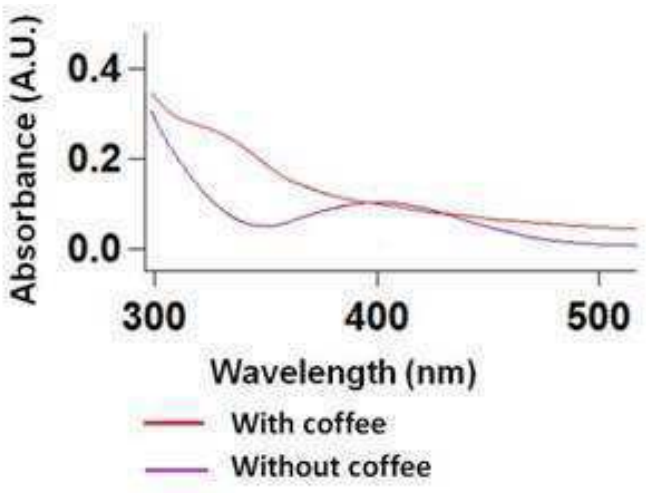

Figure 4.4: UV-Visible spectra of standard toner solution, and coffee-added toner solution.

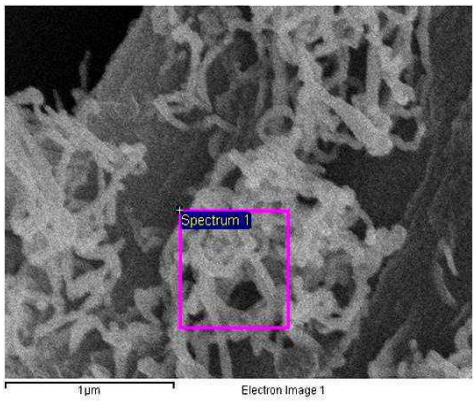

Element	Average Atomic %
Ag	92.69
Pd	0
Cl	0
Au	7.31

Figure 4.5: SEM-EDX measurements from the coffee-added toner sample fail to detect the presence of palladium.

However, when silver nanowires were dipped into this coffee-added toner solution, the presence of palladium could not be detected by EDX measurements (Fig. 4.5). We attribute this to the absence of a driving force for Pd nanoparticles to deposit onto silver nanowires from the toner solution unlike in galvanic exchange, wherein the difference in electrochemical potential drives the movement of Pd^{2+} ions onto Ag surface.

It is known that citric acid or citrate ions can adsorb on a metal surface via carboxylate groups [43]. The standard palladium toning solution has citric acid as one of its components to enhance the surface adsorption of palladium by electrostatic interactions with adsorbed carboxylate groups, and this step is a precursor to galvanic exchange. We hypothesized that the extent of surface adsorption of citrate may be negligible in the presence of coffee powder, and so, if the silver nanowire paper is pre-treated with citric acid then the adsorbed carboxylate groups can provide an electrostatic driving force to attract the palladium nanoparticles onto the silver nanowires. Based on this hypothesis, the silver samples were immersed in a 0.16 M solution of citric acid monohydrate for 3 h prior to dipping in a coffee-added toning solution. For comparison, some silver samples pre-treated with citric acid were also dipped into a solution of the original toner. The time of palladium deposition was also maintained at 3 h. Figure 4.6 shows that silvery flakes float on the top of the standard

toner solution, while such flakes were not seen on top of the coffee-added toning solution.

Figure 4.6: After 3 hours of deposition onto a citrate-activated silver nanowire sample, the cap containing the standard toner (left) shows silvery flakes floating on the surface, while the cap containing the coffee-added toner (right) does not show any flakes.

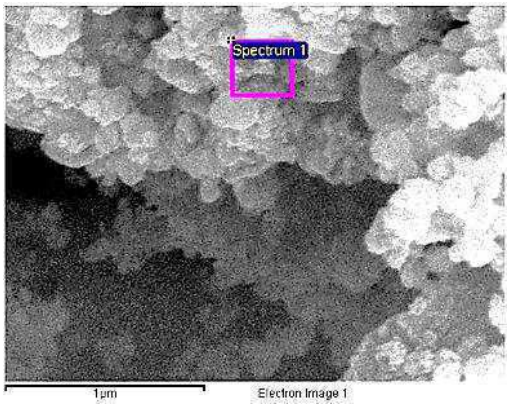

Element	Average Atomic %
Ag	52.65
Pd	19.02
Cl	23.69
Au	4.65

Figure 4.7: Representative FESEM image of the samples dipped in standard toner solution for 1 hour with the average elemental analysis for this sample

Figures 4.7 and 4.8 show representative FESEM images, as well as averaged elemental analysis, of silver nanowire samples dipped for 1 h in standard toner and coffee-added toner solutions respectively. Note: these samples were coated with a nominally 8 nm thick layer of gold to eliminate any risk of charging during FESEM imaging. The morphology of the sample dipped in standard toner is lumpy unlike that of the as-developed silver nanowires, whereas the morphology of the sample dipped in coffee-added toner is like that of the as-developed silver nanowires. This difference is attributed to the effect of galvanic displacement. Galvanic exchange gives rise to

lumpy texture owing to the large free energy difference, which results in a faster rate of silver displacement and truncation of nanowires into more spherical aggregates [44]. The EDX analysis shows the presence of palladium in both types of samples. This indicates that the additional step of activating the silver surface by dipping in citrate facilitates the deposition of palladium onto silver nanowires from the coffee-added toner solution. The EDX analysis indicates the presence of chlorine only in the sample dipped into a solution of the standard toner. The absence of chlorine signal from the sample dipped in coffee-added toner solution indicates that galvanic displacement has been avoided, as otherwise the displaced silver ion will form insoluble silver chloride and partly redeposit onto the substrate

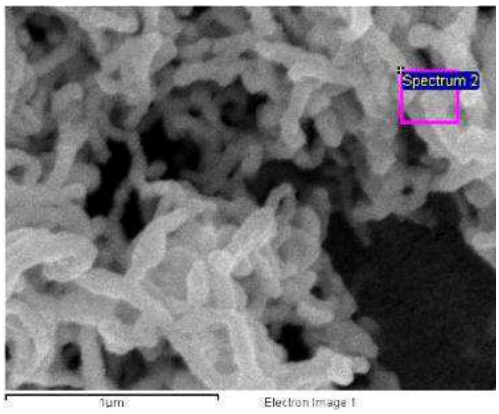

Element	Average Atomic %
Ag	70.65
Pd	23.06
Cl	0
Au	6.28

Figure 4.8: Representative FESEM image of the samples dipped in coffee-added toner solution for 1 hour with the average elemental analysis for this sample.

When normal toning is carried out for 1 hour without citric acid pre-treatment, the average elemental analysis from EDS reveals that the elemental composition is nominally similar (slightly higher value of Pd content, Table 4.1) to the composition of the sample without citric acid pre-treatment. Hence it can be seen that citric acid pre-treatment is the key to achieve Pd deposition using coffee-added toning. Citric acid adsorbs using its carboxylate groups on the surface of metals [12] and attracts palladium onto silver surface.

Table 4.1: Average elemental analysis for sample with 1 hour of normal toning without undergoing citric acid pre-treatment

Element	Average Atomic %
Ag	52.22
Pd	24.7
Cl	20.79
Au	2.29

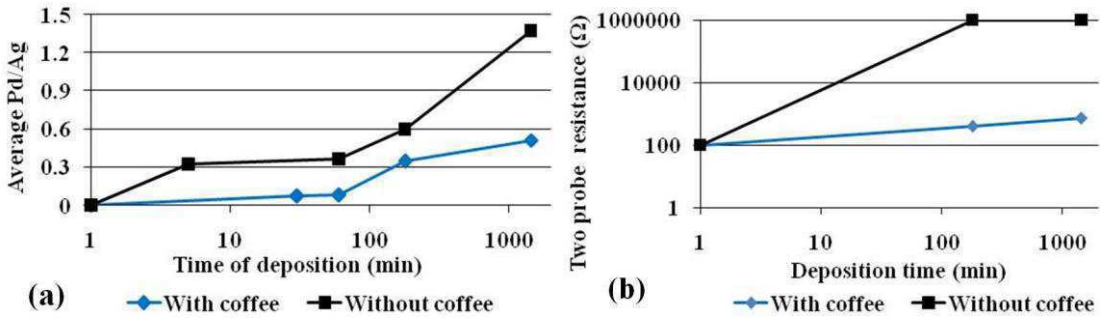

Figure 4.9: (a) Average Pd/Ag ratios of palladium deposition carried out in presence and absence of coffee for different toning times on paper. (b) Two probe resistance of some of these samples.

Palladium deposition using coffee-added toner was performed for 30, 60, 180 and 1440 minutes. Palladium deposition using standard toner was done for 5, 60, 180 and 1440 minutes. The toning was done on separate samples of silver on paper, all having the same initial electrical resistance of 20 Ω. The average Pd/Ag ratios were calculated by EDS for all of them. Figure 4.9a shows a plot of the atomic ratio of palladium to silver as a function of deposition time for samples dipped in standard

toner as well as samples dipped in coffee-added toner solution. Figure 4.9b shows the representative values of resistance measured across the edges of some of these samples. The samples toned using the coffee-added solution exhibit a slower rate of palladium deposition, but maintain their conductivity indicating that the nanowire morphology is still maintained. Whereas, the samples prepared using the standard toner rapidly lose their conductivity, which is consistent with the rounded morphology observed using FESEM. The samples toned using the standard recipe were non-conducting, having resistance in the order of 10^6 ohms, just after 3 h of toning. This is represented as "Open Loop" in the multimeter. The coffee toned samples, under the same conditions, have resistances of the order of few hundreds of ohms.

From the XPS analysis (figure 4.10), it was confirmed that palladium is predominantly present in its reduced form as Pd^0 in the case of coffee-toned Ag nanowires. The peaks observed at 335.5 eV and 340.7 eV correspond to $Pd^0_{3d5/2}$ [45] and $Pd^0_{3d3/2}$ [46] respectively. A bare Ag nanowire substrate was also characterised using XPS analysis and shows peaks at 368.04 eV and 374.04 eV that correspond to $Ag^0_{3d5/2}$ and $Ag^0_{3d3/2}$ respectively [47].

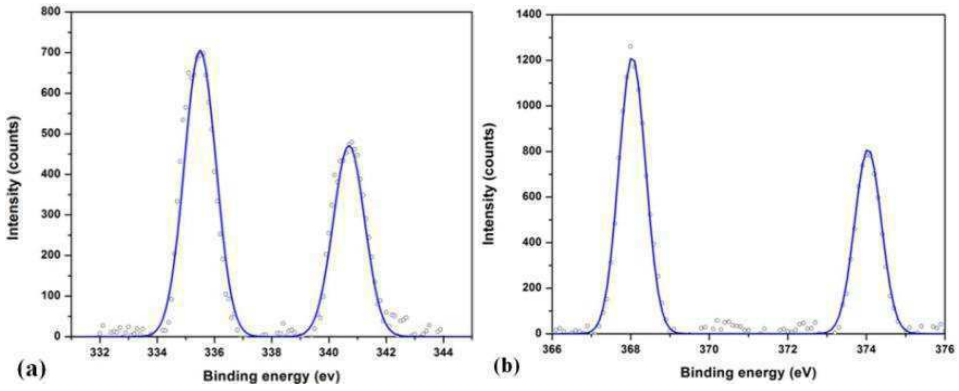

Figure 4.10: (a) XPS spectra showing palladium-3d signal for samples prepared by dipping in coffee-added toner for 1 h. (b) XPS spectra showing silver-3d signal for samples without any Pd toning

4.3 Plastic-substrate for hydrogen detection

The results discussed till now were pertaining to detecting elements developed on copier paper. It is quite easy and cheap to make such paper-based detecting elements. However, since paper was considered as a flammable hazard, alternative substrates were explored. In this report, consideration is given to commercially available

overhead transparencies. Overhead transparency sheets (PET) were selected as the substrate since they are flexible and inexpensive. Also, they have a higher ignition temperature than that of paper [48]. However, unlike paper, they cannot retain aqueous-based printing inks, in that they are hydrophobic. To make the OHP sheets hydrophilic we initially adapted a layer by layer (LBL) process developed earlier in our group [11], wherein plasma cleaning of such transparency renders the surface hydrophilic for a short time. Then by alternately dipping it in solutions of oppositely charged polyelectrolytes (poly (sodium styrene sulfonate) (PSS) and poly (diallyl dimethyl ammonium chloride) (PDDA)), a hydrophilic surface suited for printing can be obtained.

While the LBL method has its advantages in that it is quite versatile and can handle a variety of substrates, it is tedious and time-consuming, and renders only one surface hydrophilic and requires the use of plasma cleaner and some expensive chemicals. Hence, we investigated several alternative processes. Kim et al. [49] have shown a nonaqueous reaction scheme for transforming the surface of plastics from hydrophobic to hydrophilic through the use of a base-catalysed trans-esterification reaction with polyols. It is permanent, does not release contaminants, and causes no optical or mechanical distortion of the plastic.

The following processing steps were used to render the plastic surface hydrophilic and suited for inkjet printing of aqueous solutions. Small pieces of OHP sheet are cut and washed with acetone for 10 min before the reaction, just to clean the surface. Then they were placed in an ethylene glycol solution containing 10 % (w/v) KOH in an oven at 55 °C for 1 hour. Then the usual print – expose – develop process was used to obtain silver nanostructures on the plastic substrate. This process could also be carried out on a Scotch tape (figure 4.11).

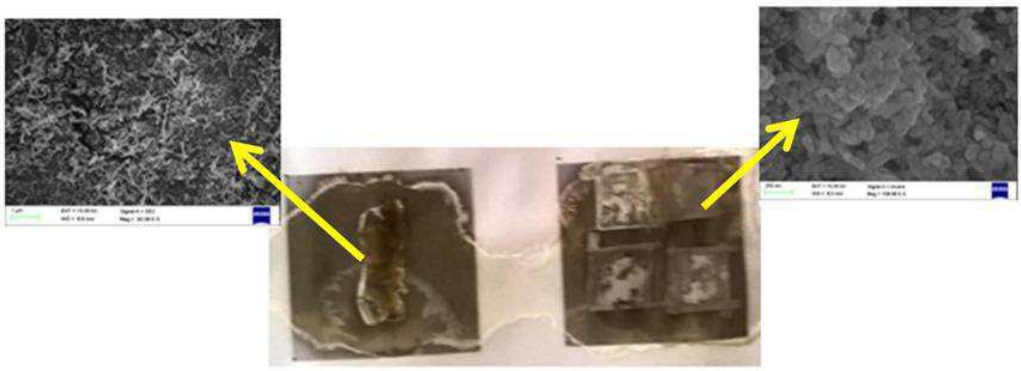

Figure 4.11: Silver nanowires printed on scotch tape (left) and OHP substrate (right), which were rendered hydrophilic by the ethylene glycol method

However, such transparency sheets are not only hydrophobic, they are also very smooth, such that even after making them hydrophilic the printed silver was also removed from the surface in the developing step. While carefully pouring the developer on such a surface, the silver would come out in the solution because of poor adhesion to the surface. Even if some part of silver remained on the surface after this step, it would quite easily be scratched out, unlike paper. This is quite undesirable for practical applications (figure 4.12).

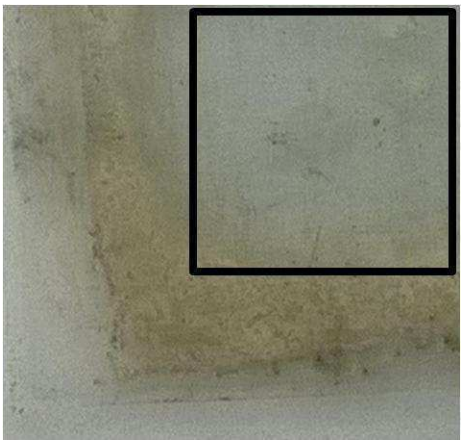

Figure 4.12: Conductive silver nano-wire network (dark region) printed on OHP treated by the ethylene glycol method washed away (boxed region) during the developing step

It was surmised that the surface roughness had a part to play in enhancing surface adhesion on paper. Hence the plastic substrates were roughened by scratching them using P220 sandpaper.

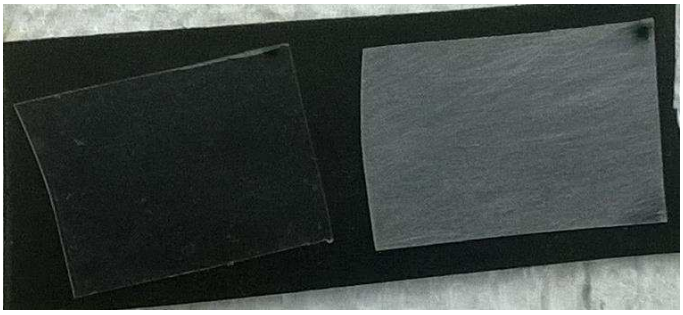

Figure 4.13: OHP before (left) and after (right) scratching with sandpaper

The sandpaper was used until the whole surface turned “white” (figure 4.13) from transparent due to scattering. These roughened-OHP sheets also exhibited sufficient wettability for inkjet printing. Such substrates were then used for printing the silver nanostructures on them. The silver nanostructures were found to be more adherent and also more scratch resistant. The roughness was characterized by optical profilometry for normal OHP samples and the ones roughened with sandpaper. The roughness maps are shown in figures 4.14 and 4.15.

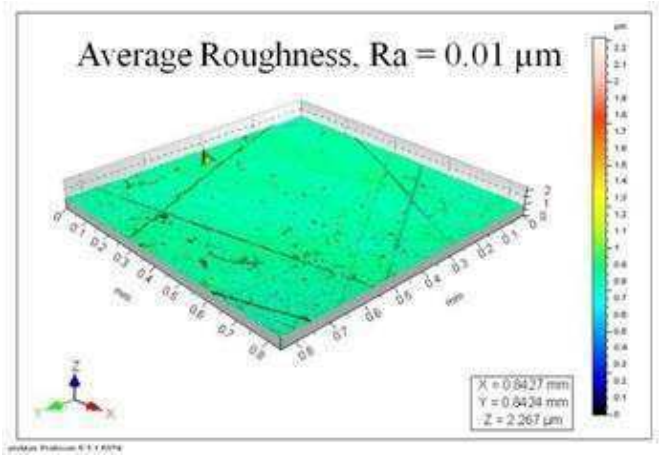

Figure 4.14: Roughness map of the OHP sheet as bought

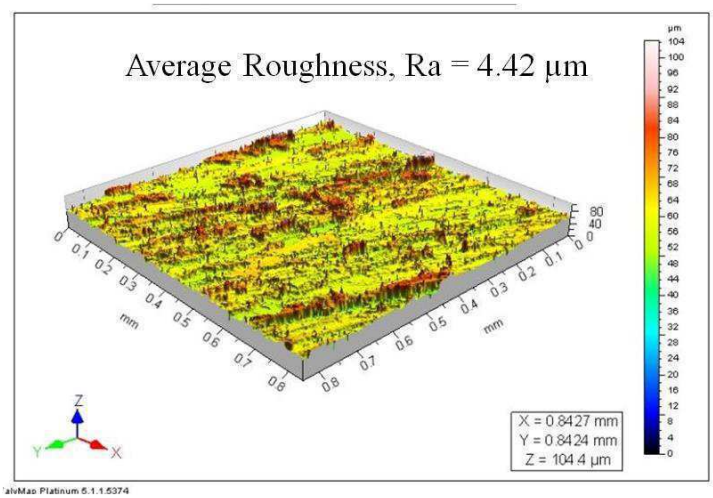

Figure 4.15: Roughness map of OHP sheet after treatment with sandpaper

Optical profilometry indicated that indeed the roughness had increased from an average value of 0.01 µm to 4.42 µm after roughening with sandpaper. This was enough to not only make the OHP surface wettable, but also provide adhesion to the printed silver pattern so that it did not wash away during the development step.

CHAPTER 5

DETECTOR TESTING

5.1 Gas sensing setups

Preliminary sensor testing was performed using the test facility in the gas sensors lab located in CeNSE, IISc. The schematic of the setup used is shown in figure 5.1,

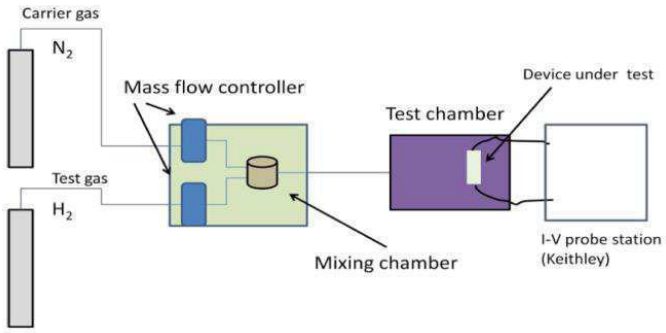

Figure 5.1: Schematic of hydrogen sensing setup at CeNSE, IISc. Reproduced from [11]

Mixing of carrier gas (nitrogen) and test gas (hydrogen) takes place in a mixing chamber. With the use of mass flow controllers, the ratio of hydrogen and nitrogen can be controlled to have a desired hydrogen concentration. This gas mixture is directed onto the test sample in the testing chamber. Recording of the response takes place simultaneously. Testing of samples, silver nanowires coated with palladium both in the presence and absence of coffee, was done one after the other. Following sequence was used to perform the test:

(i) Gas flow was avoided, and the response was recorded.

(ii) Then, only nitrogen was passed, and the response was recorded.

(iii) The flow of Hydrogen (1000 ppm) mixed with nitrogen took place for roughly the same time, and the response was recorded.

(iv) Same as (ii)

(v) Same as (i)

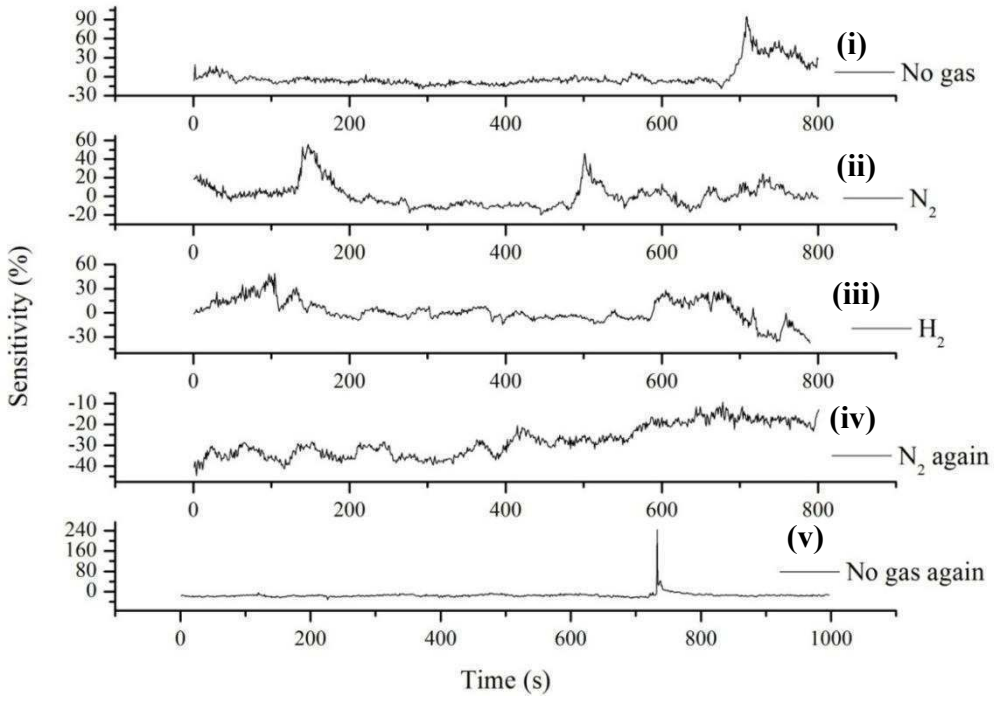

Figure 5.2a: Sensitivity vs time response for Ag-Pd detecting element fabricated using coffee-added toner.

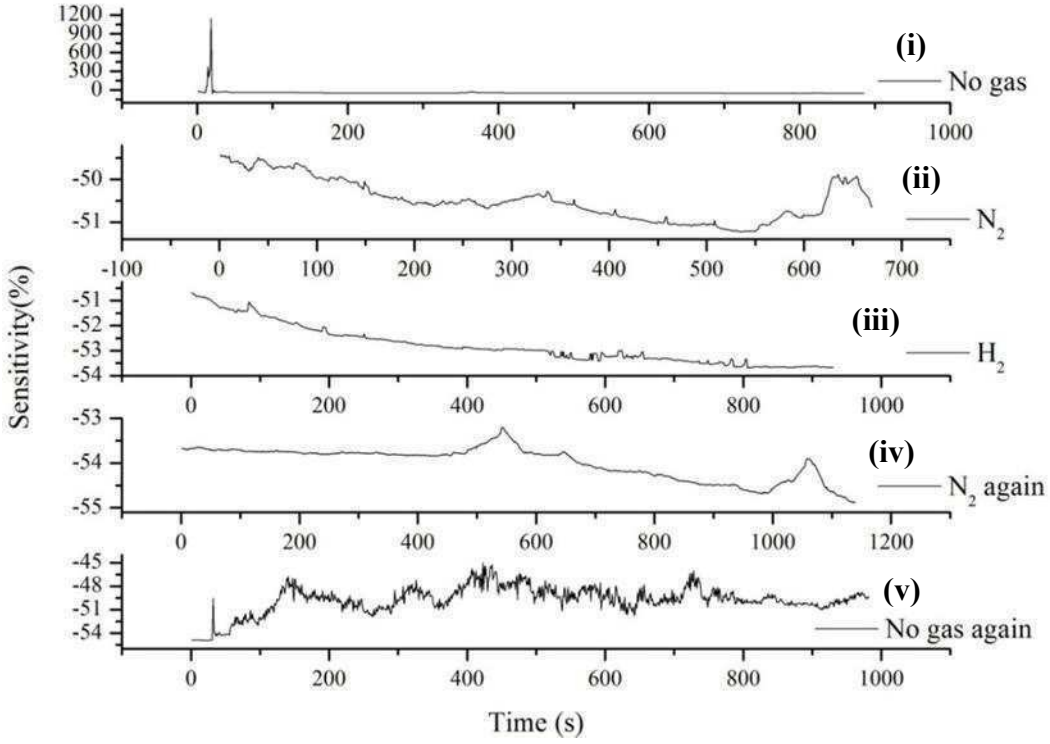

Figure 5.2b: Sensitivity vs time response for Ag-Pd detecting element fabricated using standard toner.

Figures 5.2 (a) and (b) show plots of sensitivity, i.e. $[(R-R_0)/R_0]$ *100 vs time in seconds. Here R_0 is the base resistance calculated over the first 100 readings when no gas is flowing over the detecting element. The results indicate that there is no remarkable difference in the sensor's sensitivity to exposure to 1000 ppm of hydrogen gas. Instead, there are lots of fluctuations that are not repeatable even after switching off the gas flow. Upon careful observation, we found that the setup used for sensing these elements is used for semiconductor-based sensors that have kilo to megaohms of resistance, whereas the paper-based sensing elements had a base resistance of the order of a few tens of ohms. The connecting wires from the elements used in this setup were parts of a probe station, which have much higher resistance than that of our detecting elements. As there are standard test setups for hydrogen sensing proposed by ISO guidelines [35], and as the test setup at CeNSE, IISc did not meet these guidelines, it was decided to fabricate the test setups as per ISO guidelines (see section 3.6).

5.2 Test results

Table 5.1 provides a summary of the main characteristics of the samples that were tested using the home-built flow-through setup for their response to hydrogen.

Table 5.1: Samples prepared for testing in diffusion chamber and flow though setups

Sample label	**Pd /Ag ratio, (EDX)**	**'Coffee-added'**	**Substrate**	**Base resistance R_0 (Ω)**	**Palladium deposition time (h)**	**$PdCl_2$ concentration used for toning (mM)**	**Hydrogen Dosage (H_2conc, % /time, s)**
a	0	-	Paper	17	-	-	10.7/ 360
b	0.08	Yes	Paper	29	1	4	100 / 540
c	0.32	No	Paper	248	1/2	4	10.7 / 360
d	0.51	Yes	Paper	717	24	4	10.7 / 360
e	0	-	OHP	60	-	-	10.7 / 360
f	1.06	Yes	OHP	205	24	4	10.7 / 360
g*	1.06	Yes	OHP	205	24	4	10.7 / 120
h	1	Yes	OHP	1054	168	8	10.7 / 120

* g represents a repeat measurement on sample f, for smaller exposure duration

5.2.1 Flow-through setup

The measurement of changes in resistance of the test samples subjected to various gas phase environments in the flow-through test set-up are summarised as plots of sensitivity ($\Delta R/R_0$) vs time (Figure 5.3). In these figures, the red coloured portion of the curves represent the duration during which hydrogen flow was added onto the base flow of nitrogen to achieve the desired concentration. The temperature during these tests were recorded to be 28 °C. The important observations based on the results of the flow through tests are:

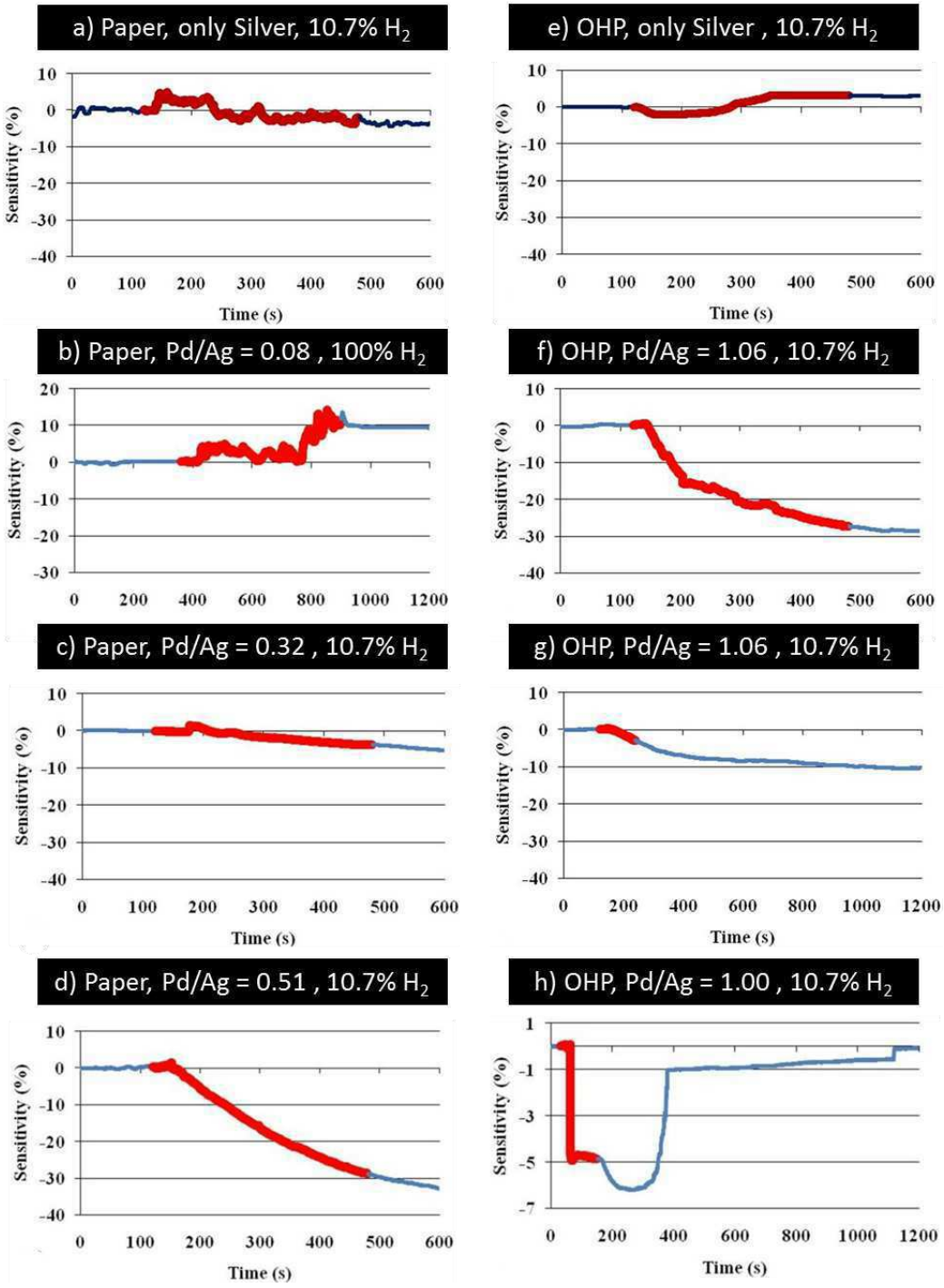

Figure 5.3: Measured responses of the various samples tested using the flow-through test setup. The red coloured portion of the curves represent the duration during which hydrogen flow was added onto the base flow of nitrogen

(i) Role of Palladium

The need for palladium to detect hydrogen is evident from figure 5.3. With palladium, the sensitivity change upon exposure to hydrogen is more prominent, monotonic and well above the noise level (root mean square value of sensitivity prior to hydrogen exposure is 0.24%, in Fig 5.3 (f)), while the sample without palladium shows random fluctuations (root mean square value of sensitivity during hydrogen exposure is 2.32%, in Fig 5.3 (e)).

(ii) Effect of palladium content

The Pd/Ag ratio as measured by EDS is an indicator of the palladium content of the detector. Pd/Ag ratio ≥ 0.32 leads to appreciable signal upon H_2 exposure. For most of the samples, the resistance drops upon exposure to hydrogen. The decrease in resistance indicates that the effect of expansion on electrical conductivity is more significant than the formation of palladium hydride. For the sample with Pd/Ag ratio of 0.08, the sensitivity fluctuated initially for about 400 s and after that showed a clear increasing trend. We conjecture that there is not sufficient palladium in the network to affect the percolation pathway by expansion, and so the response is slow and resistance increases after most of the palladium is converted to palladium hydride. Interestingly, even after switching off the hydrogen supply (base flow of N_2 was kept on), the response continues with the same decreasing trend till saturation is reached. We suppose that the plastic sealant bags act as an additional reservoir (capacitance) that limits the ability to suddenly change gas composition. This aspect needs to be investigated more thoroughly in the future.

The samples regained their base value of resistance after being exposed to ambient conditions overnight. This suggests that the desorption of hydrogen from the nanostructured palladium coated films is reversible but slow.

(iii) Effect of hydrogen dosage

To investigate the effect of total dosage of hydrogen, sample f was re-exposed (after the original resistance was regained – ca. 1 day) to the same hydrogen environment

but for a shorter duration (denoted as sample g). The change in resistance was lower for lower dosage. This suggests that the extent of hydrogen absorption into palladium determines the magnitude of the response. The time taken for saturation of signal response is similar for both samples f and g.

(iv) Effect of toning time

A comparison of the response of samples f and h indicate that the duration of toning has a significant effect on the response rate of the palladium toned samples. The Pd/Ag ratio measured using EDX was similar for the samples toned for 1 day and 1 week, while the base resistance increased from 205 Ω to 1 kΩ. Although the Pd/Ag ratios are representative of the sample they may need to be verified independently using a bulk technique. Presuming that the averaged EDX ratios are representative of the bulk composition, as the nanostructured films are less than a micron in thickness, the increase in base resistance with increased toning duration indicates that some of the silver in percolating paths are etched/displaced by palladium overlayer. This redistribution of the palladium at the junctions of the percolating network is the likely cause for the rapid response of sample h. This sample was also able to recover its base resistance value more rapidly. Such an architecture, wherein the palladium is present at the junction of percolating pathways is apt for rapid detection and provides an avenue for future detector-response optimization studies. Note: The palladium salt concentration was doubled, as a precaution, to account for any loss of activity during the one-week duration of the experiment.

5.2.2 Diffusion chamber setup

To keep the test duration short and avoid interference due to unknown leaks, a hydrogen filling time of 3 min was chosen. After this the lid was displaced and the inner chamber opened up to an atmosphere of hydrogen (corresponding to 1.62 % H_2). The response of the sample toned for one week is much faster and more robust than the sample toned for one day. This again corroborates our hypothesis about the changes in morphology of the nanostructures being optimal for hydrogen detection. The leak detection response time of sample h was estimated to be 332 s. In calculating

the response times, the lowest value of sensitivity has been used as a saturation value to get its 90% value. The time taken to reach this value starting from the time when H_2 was switched on is the response time.

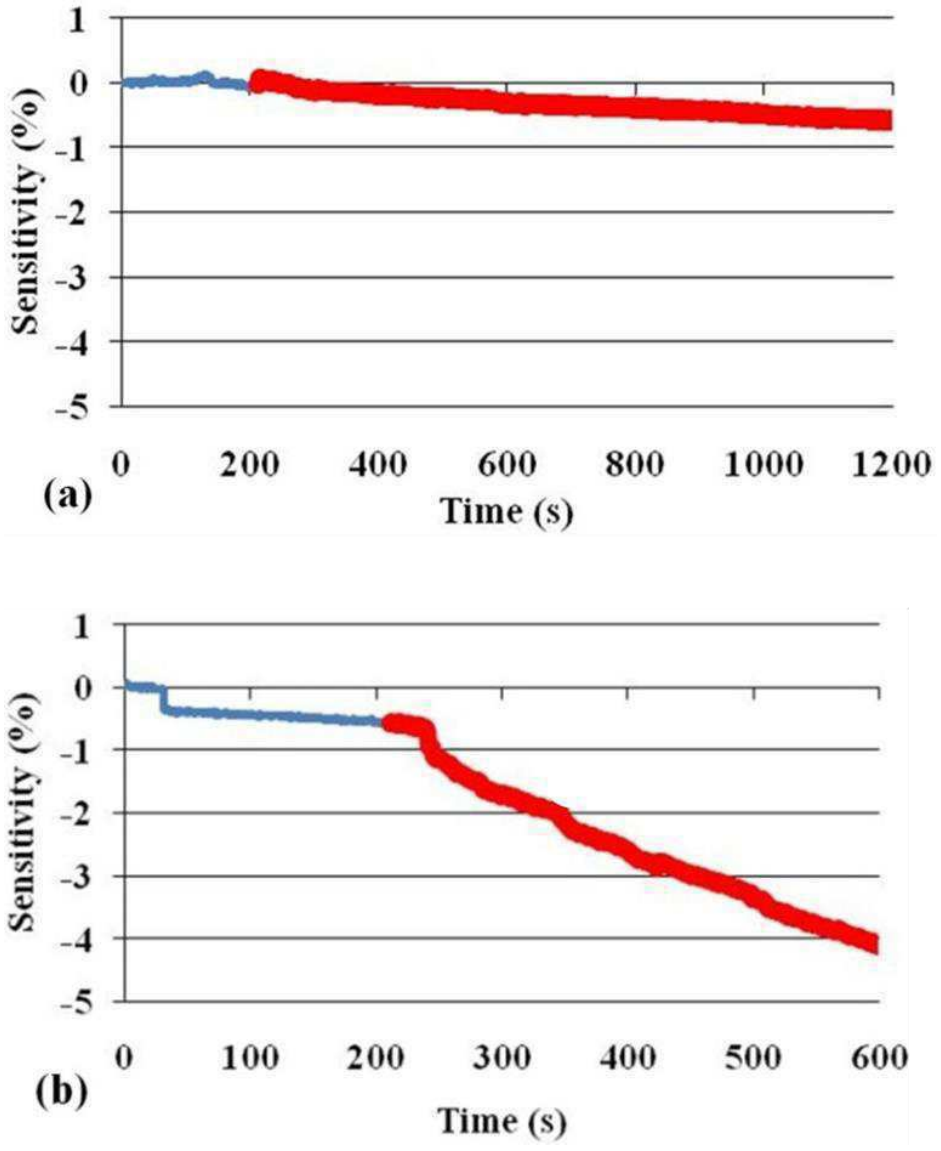

Figure 5.4: Static leak test– response of samples upon sudden exposure to an atmosphere of 1.62% H_2 (a) sample d – Pd/Ag ratio of 0.51 on paper (b) sample h – Pd/Ag ratio of 1 on OHP. The inset in (b) shows the response of the sample without palladium.

Table 5.2 compares the values observed in this study with other reports in literature using processes that can be scaled up for mass-production of palladium-based hydrogen detectors. The response time of the samples prepared in this preliminary

study are comparable to that of samples published earlier. The colour changing leak detectors employed at NASA have a reported response time of lesser than 3 min at a hydrogen concentration of 1%[10].

Table 5.2: List of Pd based detecting elements/detectors and their response time comparison with this work

Sr. No./ Year	**Detecting element/ Substrate**	**Morphology**	**Fabrication method**	**Conditions**	**t_{90} (s)**	**References**
1./(2009)	Pure Pd/ Si	Nanowires (400 nm)	Lithographic patterning	1% H_2 in N_2, RT	~250	[18]
2./(2008)	Pure Pd/Alumina	Nanowires	Electro deposition	1% H_2 in N_2, RT	~300	[18]
3./(2013)	Pd –Ag/PVC	Nanowires	Electro deposition	1% H_2 in air, RT	~150	[50]
4. /(2007)	Pure Pd/alumina	Thin film	E-beam evaporation	10% H_2 in N_2, RT	~2000	[20]
5.	**Pd-Ag/OHP**	**Nanowires**	**Coffee toning, 1 week**	**10.7% H_2 in N_2, RT**	**38**	**This report**
6.	**Pd-Ag/OHP**	**Nanowires**	**Coffee toning, 1 week**	**1.62% H_2in air, RT**	**332 s**	**This report**

CHAPTER 6

SUMMARY

Based on the observations reported in this thesis, the following conclusions can be arrived at:

1. Citric acid pre-treatment is important for ensuring uniform palladium deposition onto silver nanowires using coffee-added toner solution.

2. Coffee powder is useful for suppressing the galvanic displacement of silver by palladium during the toning step.

3. Roughness is the key for good wettability as well as excellent adhesion of printed silver nano-wires on OHP substrates. Commonly-available sandpaper can be used to roughen plastic substrates and render them amenable to inkjet printing of aqueous salt solutions.

4. The test setups to characterize the performance of detecting elements were fabricated according to the standards prescribed in ISO 26142.The salient points of the results of the preliminary experiments on hydrogen detector performance characterization are:

i. The detection mechanism is based on gap closure in samples with high palladium content, as the resistance of these samples drop after hydrogen exposure.
ii. The sample toned for one week exhibited the fastest response and had a response time of 38 s upon being exposed to a gas flow having 10.7% H_2, and 332 s upon exposure to a leakage of gas comprising of 1.62% hydrogen.

CHAPTER 7

FUTURE WORK

1. Detector recovery is one of the most important aspects to be investigated. Till now, we have seen that in all the detector response curves, recovery was not seen within 20-30 minutes of conducting the test in the 24-hour coffee toned samples. However, recovery was seen within 10 min, when the toning time was increased to 1 week. A more systematic investigation of the effect of the silver /palladium loading of the nanostructures is required to identify compositions with faster response and recovery times suitable for real-world applications.

2. Different morphology of silver nanostructures can be studied, as it is expected that the nano-gap mechanism may be more prominent in silver nanoparticles instead of silver nanowire networks.

3. Incorporation of the hydrogen detector structures into Radio frequency identification (RFID) antenna structures can help retrieve signals from the detector remotely [51]. This would be beneficial for avoiding risks to safety-personnel monitoring the hydrogen pipelines.

Appendix A

How to establish an Ethernet connection from a PC/laptop with the Keithley 6221 model

To establish the communication between Model 6221 and PC through Ethernet follow the steps below [52]:

1. On the 6221, press COMM.
2. Select Ethernet, press ENTER. 3. Now go to the PC and use the Command Prompt. Usually under Accessories or WINDOWS SYSTEM.
3. Type in IPCONFIG. And press ENTER on the keyboard.
4. Find Ethernet Adapter Ethernet.
5. Locate IPv4 address (example… 134.63.74.128). write this down.
6. Locate Subnet Mask(example… 255.255.255.0) write this down.
7. I there is a default gateway write it down (example… 134.63.74.130).
8. Go back to the Model 6221. And select IP and press ENTER.
9. Enter in the IP address in step 6, except increase the last digit by one (128 is now 129). Press ENTER.
10. Select Subnet, press ENTER.
11. Enter in the subnet mask number in step 7. (Example: 255.255.255.0). Press ENTER.
12. Select Gateway, press ENTER.
13. Enter in gateway from step 8. Increase the last digit by one (130 is now 131). Press ENTER.
14. Press EXIT twice.
15. Now back to the PC and in the command prompt, type in the word PING 134.63.74.129, press ENTER on the keyboard.
16. It should return with four replies…
17. If step 16 is good, then communication is there.

Now you can start the 6220 demo software, and it should “find” the 6221.

Appendix B

Example of program used for pulsed testing:

This is an example of the program entered in the Keithley communicator to send command to the combined 6221-2182A instrument to start the pulsed test. The program is based on the SCPI code generated by the KI6220 example software.

```
:sour:swe:abort
WAIT3000
*rst
:SYST:COMM:SERIal:SEND "SYST:FFIL ON"
:OUTP:ISH OLOW
:outp:lte OFF
WAIT500
:sour:del 0.094
:form:elem READ
:sour:pdel:high 0.004
:sour:pdel:low 0
:sour:pdel:count 30
:sour:pdel:rang best
:sour:swe:rang best
:sour:pdel:width 0.001
:sour:pdel:sdel 0.0001
:sour:pdel:swe off
:sour:pdel:lme 1
:sour:pdel:int 50
:sour:curr:comp 10
:sour:curr:start 0
:sour:curr:stop 0.01
:sour:curr:step 0.01
:SYST:COMM:SERIal:SEND ":sens:volt:rang 10"
:sens:aver:wind 0
:sens:aver:stat off
:sour:pdel:arm
WAIT3000
:init:imm
```

Use the “trace:data?” command after the test is over to get the voltage readings stored in the buffer in the Keithley communicator window.

Appendix C

Mounting the detecting element in the flow-through setup

The ISO guidelines require that the detecting element is kept in between the flanges fixed on the pipe carrying the test gas [35]. The flanges provide a platform for keeping the sensor in a fixed way. An O-ring is also kept above the detecting element to minimize the gas leakage [34]. The weight of the other flange compresses the o-ring to some extent which then seals the gaps between the flanges. The flanges used in this work have an opening in the centre which is used for screwing them on the T – junction emanating from the main pipe. It is necessary to close these openings as the gas can leak from there too. An ordinary cello tape was used for that purpose. The detecting elements developed in this work are of roughly 1 cm by 1cm dimension. The opening in the centre of the flange has a 1 in ID, which is larger than the size of such detecting elements. According to [34], the quickest and most repeatable sensing results were obtained when the area of the flange opening was same as that of the detecting element. Also, since the detecting element was to be kept in between the flanges and as well as connected to the wires of the Keithley 6221-2182A instrument, an extension coming out of the flanges was necessary to connect the both of them. Copper tape was used for this purpose. However, since the flanges were made of stainless steel and hence were electrically conducting, created a "short circuit" in that the current from the 6221 would pass through the flanges and not the detecting element, as the flanges were less resistive than the detecting element.

To avoid this situation the flanges were covered by copier paper. The paper was also cut in the central part of the flange to match the area of the detecting element. The copper tape is quite flexible and can be prone to tear if not appropriately supported. For this purpose a thick and transparent piece of polyester film was cut in the appropriate size, to be used as a sturdy base for the detecting element and the copper tape. A small part of the polyester was cut in the shape and size of the detecting element in it central part. The copper tapes were fixed on either side of the central part, where the detecting element was placed. Another smaller piece of polyester sheet was placed on top of this longer polyester base, to prevent the detecting element from moving while the flanges were screwed on the T-junction or otherwise. The U-clips were used to hold both the polyester films and the detecting element in between them in place. They also provided good contact between the copper tapes and the detecting element.

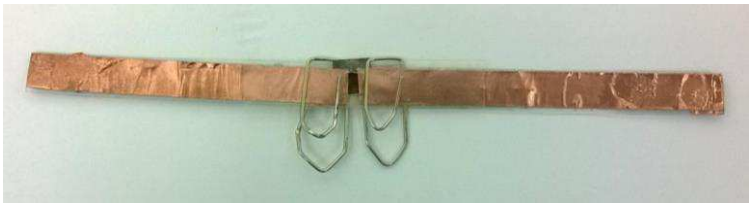

Figure C.1: Detector (between U-clips) kept in between copper tapes stuck on a flexible OHP support. U-clips provide good contact between the copper tapes and the detector

Appendix D

ATH-300 Hydrogen generator

It was found that there was a need to have a source of producing pure hydrogen gas and that too one, which does not store hydrogen gas. The Annexure A of ISO 26142 [35] describes the injection of pure hydrogen gas through the inlet of the diffusion chamber setup when the test starts. A cylinder of pure hydrogen gas was deemed to be too risky and dangerous for this sole purpose. Hence a gas generator, that can produce almost pure hydrogen gas, as and when required without storing it, was sought after.

Figure D.1: ATH-300 hydrogen generator

An ATH-300 generator was purchased from Athena Technologies, Thane, for this purpose. It produces 99.999% pure hydrogen. It produces hydrogen gas by electrolyzing a lye solution of potassium hydroxide (KOH) solution.

$$\text{Anode:} \quad 2\,OH^- \longrightarrow H_2O + \tfrac{1}{2}\,O_2 + 2\,e^-$$

$$\text{Cathode:} \quad 2\,H_2O + 2\,e^- \longrightarrow 2\,OH^- + H_2$$

$$\text{Net reaction:} \quad 2\,H_2O \longrightarrow 2\,H_2 + O_2$$

Oxygen is also produced as a by-product which is simply vented out into the environment. The hydrogen, on the other hand, is produced at the cathode and is used thereafter. Moisture is also removed from it in a column of desiccant beads to ensure that the gas exiting the generator is almost pure hydrogen. To make the lye solution 320 g of KOH (85%, SD Fine Chemicals Ltd., Mumbai) was dissolved in 1000 ml de-ionized water taken in a Borosil© glass beaker. It was then kept for ultrasonication until all the KOH pellets got dissolved. This lye solution was then poured into the lye tank of the hydrogen generator. The front of the generator was raised to about 40-degree angle for 3 times as was mentioned in the manual. This makes the air in the electrolysis cell get replaced with the lye solution entirely. Then 500 ml of de-ionized water was added in the lye tank, just to make the lye solution level in it between high (H) and low (L)

This liquid should be replaced after every 3 months; hence the date of using has to be noted. The black cap over the lye tank is removed, just so that the oxygen produced in the cell can be vented out. Then the power cord is connected to the standard power supply, and the generator is switched on. Hydrogen starts to get produced, and the display in the front panel shows the volumetric flow rate of hydrogen production. The hydrogen outlet can then be connected to a rotameter and the flow rate can be regulated.

Appendix E

Effect of dosage

The toner prepared for depositing palladium on printed silver squares is made by dissolving 7.04 mg $PdCl_2$ in 10 mL solution, which corresponds to 4.23 mg palladium in 10 mL solution. Out of this 10 mL, 2.5 mL solution is used in the caps for toning. This is equivalent to exposing 1.06 mg of palladium to 0.2 mg of silver on the sensing elements. By EDS analysis of 24-hour toned samples, it was found that the Pd:Ag ratio was slightly higher than 1:1. Hence we can assume about 0.3 mg Pd to be deposited on them.

Such sample was tested in the dosage experiment by passing 300 ml/min of H_2 for 2 minutes, i.e. 600 ml of H_2 was flown. At room temperature and pressure, since hydrogen behaves ideally, this volume corresponds to roughly 0.04 g H_2.

Hence, Mass of H_2 flown/Mass of Pd in element = 40 mg H_2/0.3 mg Pd = 133.33 mg H_2/mg Pd

As per Klotz, the maximum observed stoichiometry for absorption of H_2 by Pd was $PdH_{0.7}$ [53]. This corresponds to a weight ratio of H_2 to Pd of 0.006 mg H_2/mg Pd, that can be achieved at maximum.

The H_2 that was passed in our dosage tests was more than this value, which means that there is more than enough H_2 even for 2 minutes of H_2 flow, let alone 6 minutes. Although $H_2$was passed in excess, the sensitivity kept dropping even post switching off H_2. The reason can be a quest for the future.

REFERENCES

(1) Jacobson, M. Z. Cleaning the Air and Improving Health with Hydrogen Fuel-Cell Vehicles. *Science* **2014**, *1901* (2005), 1901–1905. https://doi.org/10.1126/science.1109157

(2) Liekhus, K. J.; Zlochower, I. A.; Cashdollar, K. L.; Djordjevic, S. M.; Loehr, C. A. Flammability of Gas Mixtures Containing Volatile Organic Compounds and Hydrogen. *J. Loss Prevent. Proc.* **2000**, *13* (3–5), 377–384. https://doi.org/10.1016/S0950-4230(99)00034-0

(3) Najjar, Y. S. H. *Hydrogen Safety: The Road toward Green Technology*; Elsevier Ltd, **2016**. https://doi.org/10.1016/j.ijhydene.2013.05.126

(4) Hübert, T.; Boon-Brett, L.; Buttner, W. J. Hydrogen Sensors In *Sensors for Safety and Process Control in Hydrogen Technologies*, Jones, B., Huang, H., Eds.; CRC Press, Boca Raton, Florida, **2006,** pp 71 - 155

(5) Hübert, T.; Boon-Brett, L.; Black, G.; Banach, U. Hydrogen Sensors - A Review. *Sensor Actuat B-Chem.* **2011**, *157* (2), 329–352. https://doi.org/10.1016/j.snb.2011.04.070

(6) Watson, J. The Tin Oxide Gas Sensor and Its Applications. *Sensor Actuator* **1984**, *5* (1), 29–42. https://doi.org/10.1016/0250-6874(84)87004-3

(7) Momirlan, M.; Veziroglu, T. N. The Properties of Hydrogen as Fuel Tomorrow in Sustainable Energy System for a Cleaner Planet. *Int J Hydrogen Energ,* **2005**, *30* (7), 795–802. https://doi.org/10.1016/j.ijhydene.2004.10.011

(8) Soundarrajan, P.; Schweighardt, F. Hydrogen Sensing and Detection. In *Hydrogen Fuel: Production, Transport and Storage*, Gupta R. B., Eds.; CRC Press, Boca Raton, Florida, **2008**, pp 495–534.

(9) Buttner, W. J., Burgess, R. M., Schmidt, K., Hartmann, K. S., Wright, H., Weidner, E., Cebola, R., Bonato, C., & Moretto, P. Hydrogen Safety Sensor Performance and Use Gap Analysis. In *(No. NREL/CP-5400-68773). National Renewable Energy Lab.(NREL), Golden, CO (United States).*; 2017.

(10) Hydrogen Detection Tape Saves Time, Lives

https://www.nasa.gov/feature/hydrogen-detection-tape-saves-time-lives (accessed Jul 21, 2018).

(11) Joshi, P. Inkjet Printed Nanostructured Metallic Films on Flexible Substrates - A Versatile Platform for Sensing Applications, Ph.D Thesis, Indian Institute Of Science (IISc), Bengaluru, 2017.

(12) Zhang, L.; Zhu, S.; Chang, Q.; Su, D.; Yue, J.; Du, Z.; Shao, M. Palladium-Platinum Core-Shell Electrocatalysts for Oxygen Reduction Reaction Prepared with the Assistance of Citric Acid. *ACS Catal.* **2016**, *6* (6), 3428–3432. https://doi.org/10.1021/acscatal.6b00517

(13) Morsbach, E.; Kunz, S.; Bäumer, M.; Brauns, E.; Lang, W. A Fast and Sensitive Catalytic Gas Sensors for Hydrogen Detection Based on Stabilized Nanoparticles as Catalytic Layer. *Sensor Actuat B-Chem,* **2014**, *193*, 895–903. https://doi.org/10.1016/j.snb.2013.11.048

(14) Banach, U.; Castello, P.; Moretto, P.; Hübert, T.; Boon-Brett, L.; Bousek, J.; Black, G. Identifying Performance Gaps in Hydrogen Safety Sensor Technology for Automotive and Stationary Applications. *Int J Hydrogen Energ,* **2009**, *35* (1), 373–384. https://doi.org/10.1016/j.ijhydene.2009.10.064

(15) Hydrogen sensor, http://i.imgur.com/haVHNA0.jpg (accessed Jan 12, 2017).

(16) Shim, Y.S., Jang, B., Suh, J.M., Noh, M.S., Kim, S., Han, S.D., Song, Y.G., Kim, D.H., Kang, C., Jang, H. W., Lee, W.. Nanogap-Controlled Pd Coating for Hydrogen Sensitive Switches and Hydrogen Sensors. *Sensor Actuat B-Chem,* **2018**, *255* (1), 1841–1848. https://doi.org/10.1016/j.snb.2017.08.198

(17) Roberson, L., Captain, J., Williams, M., Smith, T., Tate, L; and Raissi, A., Robust , Simple , and Easy-to-Detect , Color-Changing Hydrogen Sensors In *Composite Materials; Chemistry and Materials (General)*, NIAC Symposium; 27-29 Jan. 2015; Cocoa Beach FL; United States **2009**

(18) Noh, J. S.; Lee, J. M.; Lee, W. Low-Dimensional Palladium Nanostructures for Fast and Reliable Hydrogen Gas Detection. *Sensors* **2011**, *11* (1), 825–851. https://doi.org/10.3390/s110100825

(19) Lee, J.; Shim, W.; Noh, J. S.; Lee, W. Design Rules for Nanogap-Based Hydrogen Gas Sensors. *ChemPhysChem* **2012**, *13* (6), 1395–1403. https://doi.org/10.1002/cphc.201200014

(20) Wang, M.; Feng, Y. Palladium-Silver Thin Film for Hydrogen Sensing. *Sensors Actuat B-Chem.* **2007**, *123* (1), 101–106. https://doi.org/10.1016/j.snb.2006.07.030

(21) Knapton, A. G. Palladium Alloys for Hydrogen Diffusion Membranes: A Review of High Permeability Materials. *Platin. Met. Rev.* **1977**, *21* (2), 44–50.

(22) Hunter, J. B. A New Hydrogen Purification Process. *Platin. Met. Rev.* **1960**, *4* (4), 130–131.

(23) Shamsuddin, M. Hydrogen Interaction in Palladium Alloys. *J. Less-Common Met.* **1989**, *154* (2), 285–294. https://doi.org/10.1016/0022-5088(89)90214-2

(24) Nakatsuji, H.; Hada, M. Interaction of a Hydrogen Molecule with Palladium. *J. Am. Chem. Soc.* **1985**, *107* (26), 8264–8266. https://doi.org/10.1021/ja00312a078

(25) Bartczak, W. M.; Stawowska, J. Interaction of Dihydrogen with Transition Metal (Pd, Ni, Ag, Cu) Clusters. *Struct. Chem.* **2004**, *15* (5), 447–459. https://doi.org/10.1023/B:STUC.0000037902.93420.28

(26) A., V.; G., D.; Grbovic, J.; M., D. Hydrogen Economy: Modern Concepts, Challenges and Perspectives. *Hydrog. Energy - Challenges Perspect.* **2012**, No. June 2014. https://doi.org/10.5772/46098

(27) Tanaka, S., Clewley, J.D and Flanagan, T.B. Kinetics of Hydrogen Absorption by Lanthanum-Nickel ($LaNi_5$). *J. Phys. Chem.* **1986**, *34* (2), 817–822. https://doi.org/10.1021/j100532a017

(28) Pundt, A.; Kirchheim, R. Hydrogen in Metals : Microstructural Aspects, *Annu Rev Mater Res*, **2006**, 36, 555 - 608. https://doi.org/10.1146/annurev.matsci.36.090804.094451

(29) Fukai, Y.; Sugimoto, H. Formation Mechanism of Defect Metal Hydrides Containing Superabundant Vacancies, *J Phys-Condens Mat,* **2007**, 19 (43) https://doi.org/10.1088/0953-8984/19/43/436201

(30) Otterson, D.A. and Smith. R. J., Electrical Resistivity of PdHx System for H/Pd Atom Ratios to 0.97, **1970**, *J Phys Chem Solids* Vol. 31. 187-189

(31) Sakamoto, Y.; Takai, K.; Takashima, I.; Imada, M. Electrical Resistance Measurements as a Function of Composition of Palladium - Hydrogen(Deuterium) Systems by a Gas Phase Method, *J Phys-Condens Mat,* **1996**, 8 (19). https://doi.org/10.1088/0953-8984/8/19/015

(32) Ward, T. L.; Dao, T. Model of Hydrogen Permeation Behavior in Palladium Membranes. *J. Memb. Sci.* **1999**, *153* (2), 211–231. https://doi.org/10.1016/S0376-7388(98)00256-7

(33) Yang, F.; Kung, S. C.; Cheng, M.; Hemminger, J. C.; Penner, R. M. Smaller Is Faster and More Sensitive: The Effect of Wire Size on the Detection of Hydrogen by Single Palladium Nanowires. *ACS Nano* **2010**, *4* (9), 5233–5244. https://doi.org/10.1021/nn101475c

(34) Boon-Brett, L.; Black, G.; Moretto, P.; Bousek, J. A Comparison of Test Methods for the Measurement of Hydrogen Sensor Response and Recovery Times. *Int. J. Hydrogen Energ* **2010**, *35* (14), 7652–7663. https://doi.org/10.1016/j.ijhydene.2010.04.139

(35) Hydrogen Detector: ISO/TC 197, WG 13 DIS 26142.

(36) Naoya SAWAGUCHI, Maiko NISHIBORI, Kazuki TAJIMA, Woosuck SHIN, Noriya IZU, N. M. and I. M. Practical Test Methods for Hydrogen Gas Sensor Response Chracterization. *Electrochemistry* **2006**, *74* (4), 315–320. https://doi.org/10.5796/electrochemistry.74.315

(37) Keithley 6220/6221 AC and DC Current Source User's Manual. **2005**,

(38) Keithley. Model 2182A Nanovoltmeter Datasheet. Keithley Instruments, Inc

(39) Photographic print toning, https://sheying.sioe.cn/yanlun/8956.html (accessed Dec 13, 2017).

(40) King, S. Kallitype process, http://sandykingphotography.com/resources/technical-writing/the-kallitype-process (accessed May 10, 2017)..

(41) Nadagouda, M. N.; Varma, R. S. Green Synthesis of Silver and Palladium Nanoparticles at Room Temperature Using Coffee and Tea Extract. *Green Chem.* **2008**, *10* (8), 859. https://doi.org/10.1039/b804703k

(42) Wang, Z.; Yan, J.; Wang, H.; Ping, Y.; Jiang, Q. Pd / C Synthesized with Citric Acid : An Efficient Catalyst for Hydrogen Generation from Formic Acid / Sodium Formate — Supplementary Information (B). 1–10, *Sci Rep - UK 2,* **2012**

(43) Xiong, Y.; McLellan, J. M.; Yin, Y.; Xia, Y. Synthesis of Palladium Icosahedra with Twinned Structure by Blocking Oxidative Etching with Citric Acid or Citrate Ions. *Angew. Chemie - Int. Ed.* **2007**, *46* (5), 790–794. https://doi.org/10.1002/anie.200604032

(44) Canlier, A.; Volkan, U. Development of Highly Transparent Pd- Coated Ag Nanowire Electrode via Controlled Galvanic Displacement Reaction. **2014**, 475–487. https://doi.org/10.1016/j.apsusc.2015.04.017

(45) Kumar, G.; Blackburn, J. R.; Albridge, R. G.; Moddeman, W. E.; Jones, M. M. Photoelectron Spectroscopy of Coordination Compounds. II. Palladium Complexes. *Inorg. Chem.* **1972**, *11* (2), 296–300. https://doi.org/10.1021/ic50108a020

(46) Militello, M. C.; Simko, S. J. Elemental Palladium by XPS. *Surf. Sci. Spectra* **1994**, *3* (4), 387–394. https://doi.org/10.1116/1.1247783

(47) Kaushik, V. K. Xps Core Level Spectra And Auger Parameters For Some Silver Compounds. *J. Electron Spectros. Relat. Phenomena* **1991**, No. 56, 273–277. https://doi.org/10.1016/0368-2048(91)85008-H

(48) Autoignition Temperature. *From wikipedia, accessed 31/12/2016*. https://doi.org/10.1016/b978-0-7506-1180-0.50009-x

(49) Kim, S.; Bowen, R. A. R.; Zare, R. N. Transforming Plastic Surfaces with Electrophilic Backbones from Hydrophobic to Hydrophilic. *ACS Appl. Mater. Interfaces* **2015**, *7* (3), 1925–1931. https://doi.org/10.1021/am507606r

(50) Fournier, C.; Rajoua, K.; Doublet, M. L.; Favier, F. Palladium-Silver Mesowires for the Extended Detection of H2. *ACS Appl. Mater. Interfaces* **2013**, *5* (2), 310–

318. https://doi.org/10.1021/am302143m

(51) Lee, J. S.; Oh, J.; Jun, J.; Jang, J. Wireless Hydrogen Smart Sensor Based on Pt/Graphene-Immobilized Radio-Frequency Identification Tag. *ACS Nano* **2015**, *9* (8), 7783–7790. https://doi.org/10.1021/acsnano.5b02024

(52) How to set up Ethernet Connection https://www.tek.com/support/faqs/how-set-ethernet-connection-keithley-6221 (accessed Jan 12, 2018).

(53) Klotz, E.; Mattson, B. Hydrogen and Palladium Foil: Two Classroom Demonstrations. *J. Chem. Educ.* **2009**, *86* (4), 465. https://doi.org/10.1021/ed086p465

Mechanical sensors

Strain-Sensitive Inkjet-Printed Nanoparticle Films on Flexible Substrates

Pushkaraj Joshi and Venugopal Santhanam

Department of Chemical Engineering, Indian Institute of Science, Bangalore 560012, India

Manuscript received December 20, 2017; revised January 16, 2018; accepted January 23, 2018. Date of publication January 26, 2018; date of current version February 21, 2018.

Abstract—Patterned metal nanostructured films on plastic substrates can be used as the active elements of flexible strain sensors. Herein, we report the adaptation of an inkjet-based process for the room temperature fabrication of silver nanoparticle-based strain-sensitive films on Polyethylene terephthalate (PET) substrates with a gauge factor (g) of 25 and a negligible temperature coefficient of resistance. The process is also readily extended to latex substrates for human motion detection.

Index Terms—Mechanical sensors, flexible strain sensors, human motion detection, inkjet printing, nanoparticle.

I. INTRODUCTION

Bonded foil strain gauges are commercially available for low-cost mechanical sensing applications requiring flexibility. These gauges are fabricated by etching metallic foils and have resistances in the 100–1000 Ω range for minimizing electrical interferences, especially during dynamic measurements [1]. Additive fabrication of patterned metal nanostructures on flexible Polyethylene terephthalate (PET) sheets is an attractive alternative to etching, with literature reports on touch sensors, flexible electrodes, chemiresistors, and strain sensors [2]–[6]. Typically, patterning of metal nanostructures is carried out using colloidal solutions of nanoparticles as feed material for techniques such as drop casting, Mayer rod coating, inkjet printing and convective self-assembly [3]. Amongst these, inkjet printing is sought after [1], [3] for its additive nature and amenability to roll-to-roll production. However, the need to formulate inks with additives for stable droplet formation and the need for post-processing steps to sinter colloidal inks [4], [5] hinder the commercialization of inkjet printing method. Of late, some novel strategies for room-temperature, self-sintering inks have been reported [2], [10], [11].

Recently [12], our group had demonstrated the use of a "print-expose-develop process," using a desktop inkjet printer, which obviates the requirement for ink formulation as well as subsequent sintering, while enabling the formation of flexible conductive films of silver nanowires *in-situ* on paper substrates. During bending tests these percolating silver nanowire networks did not change their resistance, which is useful for applications requiring flexible conductors. However, there is scope for developing such a desktop fabrication process to form nanostructured metal films that are sensitive to strain. For adapting this process to plastic substrates, the poor wettability of water on the PET film has to be overcome. Layer-by-layer (LbL) assembly of polyelectrolyte (PEL) films on PET substrates can help to alleviate adhesion issues [13]. In this article, we describe the successful adaptation of "print-expose-develop" process in conjunction with LbL assembly to fabricate strain-sensitive nanoparticle films on flexible PET substrates and further demonstrate the ability to carry-out human motion detection.

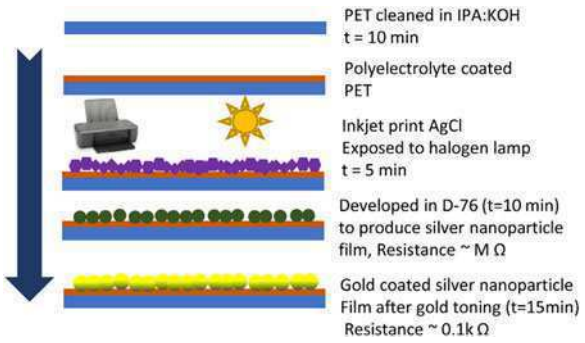

Fig. 1. Schematic of the steps involved in the fabrication process.

II. METHODS

A. Materials

Silver nitrate, potassium chloride, sodium chloride, potassium hydroxide and isopropyl alcohol were of AR grade and purchased from SD Fine Chemicals. Gold chloride (>99% purity, Alfa Aesar), Polycation – [poly(diallyl dimethyl ammonium chloride)] PDDA (M.Wt. −100 000–200 000; 20 wt.% in water, Sigma) and polyanion [poly(sodium styrene sulfonate)] PSS (M.Wt. −70 000, Sigma) were used as received. Developer D-76 was prepared as reported in the literature [14]. Gold toning solution, for gold coating of the silver surface, was prepared as described elsewhere [15]. PET sheets, 175 μm thick (Novajet), were procured locally. HP (J1100) Deskjet printer with 802 cartridges was used for printing precursor salt solutions. Metal-foil based commercial strain gauges (YFLA-5, gauge factor ~2.1, TML, Japan) bonded to a PET sheet and having 5 mm gauge length were used to calibrate the bending strain setup.

B. Fabrication Protocol

A schematic of the fabrication process is shown in Fig. 1. The polyelectrolyte coating process was adapted from literature [16]. Briefly, 1 g/L of PDDA and 2 g/L of PSS were prepared in 1.5 M NaCl

Corresponding author: Venugopal Santhanam (e-mail: svgpal@iisc.ac.in).
Associate Editor: K. Shankar.
Digital Object Identifier 10.1109/LSENS.2018.2798643

solution in DI water. The PET substrates were cleaned using a mixture of isopropyl alcohol and 1 N KOH (60:40) for 10 min and rinsed in water and then exposed to UVO Cleaner (Jelight, UV-28 mW/cm^2) for 10 min. The cleaned PET substrates were then dipped in PDDA and PSS solutions alternately for 15 min each to deposit three bilayers and finally capped with a PDDA layer. The print-expose-develop process was adapted from our earlier report [14], but with the halide composition changed from bromo-iodide to chloride species. Briefly, 0.1 M silver nitrate and 0.2 M potassium chloride solutions were alternately printed onto PEL coated PET sheets in a desired pattern and exposed to halogen lamp (500 W, 9500 Lumens) for 5 min, followed by immersion in the photographic developer (D-76) for 10 min. The developed samples were then dipped in gold toning solution for 15 min followed by rinsing in DI water and drying.

C. Material Characterization

Field emission scanning electron microscope (FESEM) images were recorded with SE2 (Everhart Thornley) detector (Zeiss, Ultra 55). EDAX-SEM analysis was performed using EDAX attachment (Oxford Instruments). XRD analysis was performed using a Rigaku SmartLab instrument with Cu-Kα radiation source. Goniometer OCA20 from DataPhysics was used for sessile drop contact angle measurements. Cr/Au (10/90 nm) electrodes with a gap of 5 mm were shadow deposited on nanoparticle films for electrical measurements. Nitrogen cooled low-temperature probe station with Agilent device analyzer model B1500A was used to measure temperature-dependent resistance.

D. Electromechanical Response Characterization

The electromechanical response was characterized using a home-built, calibrated setup along with Keithley 4200-SCS and LabView instruments (see Fig. 2). The bending test setup consisted of a fixed plate and a movable plate that could be translated using a stepper-motor controlled by a driver. The test sample was held between two plates and fixed firmly by a clamping plate on roller support. The stepper-motor driver was interfaced with LabView 7.1 software via NI DAQ card to provide GUI control. Keithley SMUs were connected to the clamp with adhesive copper tape to ensure better electrical contact with the test strain gauge. Fig. 2(b) shows the calibration curve for bending strain as a function of lateral displacement of the movable plate using the commercial strain gauges.

III. RESULTS AND DISCUSSION

A. Sensor Fabrication

After PEL coating, the water contact angle of the PET substrate decreased from 78.7° ± 1.6° to 46.4° ± 2.4°. The surface roughness after PEL coating was ~16 nm (RMS value from AFM scans). The *in-situ* reactive precipitation of AgCl film on PEL coated PET substrate was confirmed by indexing of XRD diffractogram (Fig. 3(a), ICSD – 064734). The formation of metallic silver, after light exposure and development, was also confirmed by indexing of XRD diffractogram (Fig. 3(b), ICSD – 064994). The broad peaks observed in these diffractograms are attributed to the PET substrate. Representative FE-SEM images highlight the formation of silver films with nanoparticle

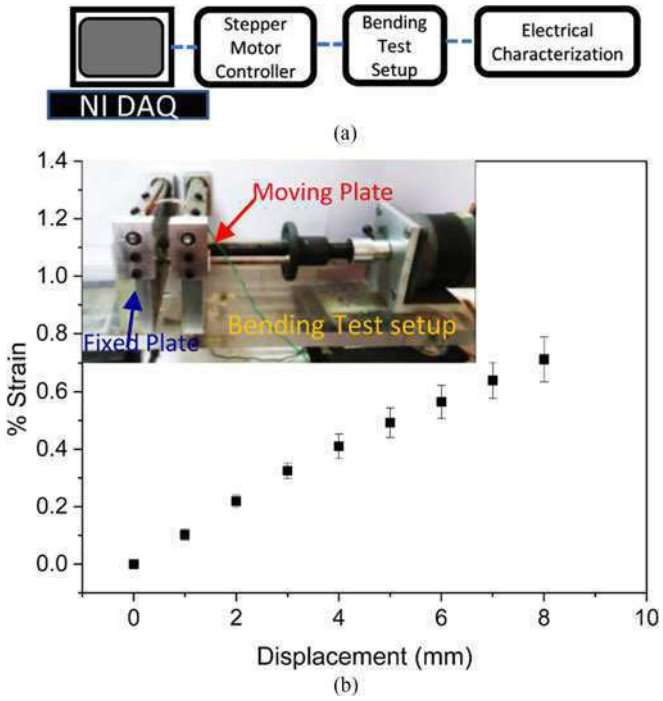

Fig. 2. (a) Schematic of set-up used for strain sensor response characterization. (b) Calibration curve of the bending test setup. The error bars are based on repeated measurements of commercial gauge made in triplicate. (Inset) Digital photograph of the test setup.

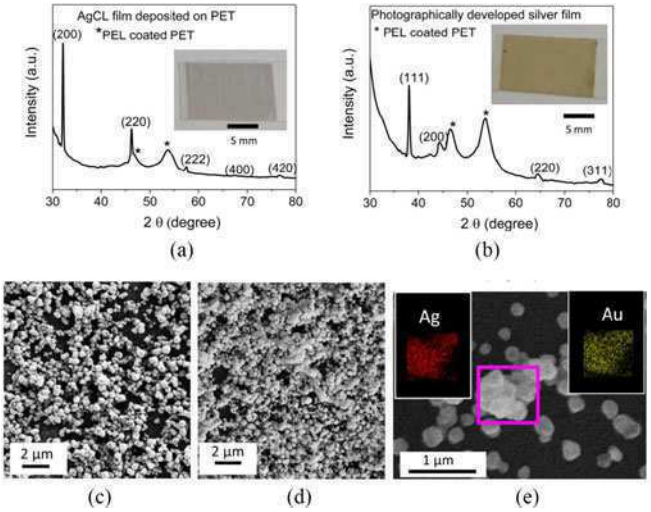

Fig. 3. XRD diffractograms of (a) undeveloped silver chloride film and (b) photographically developed silver films. The insets show corresponding photographs. Representative FESEM images of nanostructures (c) before and (d) after gold-toning. (e) Gold-coated silver nanoparticles on a silicon substrate. Insets show EDAX mapping of silver and gold from the outlined region.

morphology [see Fig. 3(c)] unlike the interconnected silver nanowire morphology obtained by starting with silver bromo-iodide films [12]. The interconnected silver nanowire films functioned as flexible conductors that did not respond to strain, but we expected the nanoparticle morphology with fewer interconnections to be more sensitive to applied strain. In pursuit of this goal, we systematically varied the silver loading from 0.1 to 0.5 mg/cm^2 of substrate by changing the

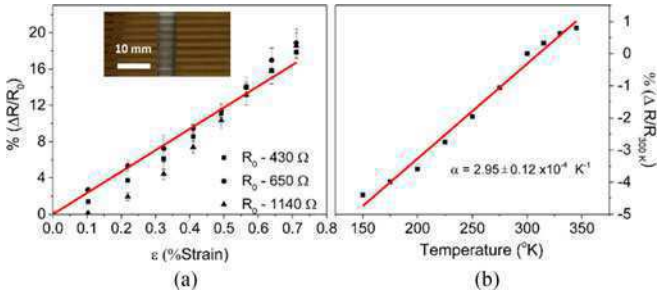

Fig. 4. (a) Electromechanical response of three test samples to bending strain. The solid line represents a fit to the average strain response. (Inset) Photograph of one such sample. (b) Relative variation of initial resistance as a function of temperature.

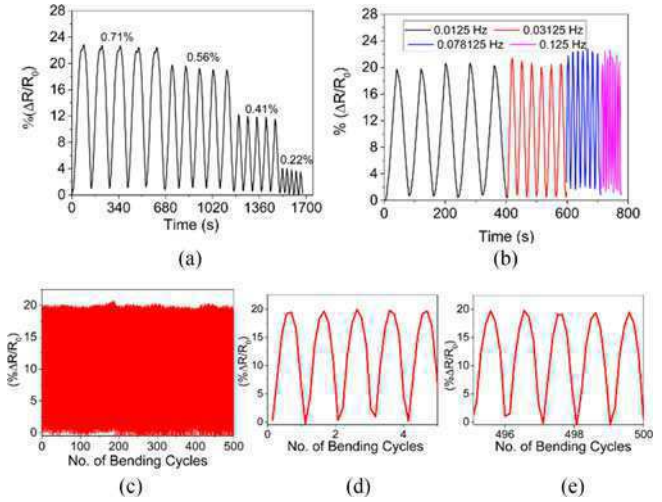

Fig. 5. Dynamic strain response characterization. (a) Variation in amplitude at a fixed frequency. (b) Variation in frequency at a fixed amplitude. (c) Robustness of response over 500 bending cycles along with a magnified view of (d) first five cycles and (e) last five cycles.

number of print cycles. However, partial desorption of the silver chloride film was observed during development, which is attributed to the solubility of silver chloride in the developer solution. This restricted the maximum value of silver loading feasible. Thus, the silver loading was fixed at 0.19 mg/cm^2 for all experiments. For fabricating strain-sensitive nanoparticle films on PET sheets, silver chloride films were printed on PEL coated PET sheets with the desired number of parallel lines having linewidth ~900 μm, gap ~1 mm, and a nominal silver loading of 0.19 mg/cm^2. However, these silver nanoparticle films were significantly resistive and prone to tarnishing over time. Therefore, a coating of metal to enhance conductivity and stability was sought. Pursuant to the theme of silver halide photography, plating of gold was carried out using a gold-protective solution (GP-2), which is used for providing blue tones and for avoiding the tarnishing of silver photographs [15]. Gold toning resulted in a drop in the resistance of the samples to hundreds of ohms, which is typical for commercially available metallic strain gauges. A comparison of FESEM images [see Fig. 3(c) and (d)] shows that the morphology of gold-coated silver nanoparticle films is like that before gold toning, which is suggestive of a uniform coating. For evaluation of the extent of gold coating using EDAX, photographically developed silver nanoparticles on silicon wafer substrate were immersed in gold toning solution to avoid issues with charging and drift on PET substrates during the time required for EDAX signal collection. The elemental maps [see Fig. 3(e)] of silver and gold further confirm the uniformity of the gold coating.

B. Electromechanical Response

Electromechanical testing was carried out on samples having different initial resistances, obtained by varying the number of parallel lines. All the devices tested exhibited a linear response to bending strain [see Fig. 4(a)], giving rise to an average gauge factor of 25 [defined as per (1)].

$$\frac{\Delta R}{R_0} = g\varepsilon \tag{1}$$

where R_0 is the initial resistance of the device, ΔR is the change in resistance, ε is the applied strain, and g is the gauge factor. The sensor resolution is estimated to be $4 \times 10^{-4}\varepsilon$, based on the prediction band of the fit.

The gauge factor is ~10 times higher than commercially available metal film-based strain gauges. These results are comparable to the values of gauge factors (strain range) reported in the literature {2.5 (0.3%) [6], 8 (1%) [5], 50 (0.8%) [17], 17 (0.022%) [4], and 100 (0.7%) [18]} for metallic nanostructured films. A salient factor of this work is the lower base resistance (comparable to commercial strain gauges) of the order of 0.1 kΩ in contrast to the earlier reports on samples having MΩ resistance. The applied strain results in an increase in the inter-cluster distance along the nanoparticle film. The higher strain-sensitivity of the nanoparticle film is attributed to the tunnelling junctions present in the percolating pathway of the nanoparticle film. The presence of parallel pathways with different gap widths averages out the exponential response over this strain range, making it linear. Furthermore, the value of the temperature coefficient of resistance (TCR ~$2.95 \pm 0.12 \times 10^{-4}$ K^{-1}) of gold-toned silver nanoparticle films [see Fig. 4(b)] is comparable to that of typical alloys used for strain gauge fabrication and ~10 times lower than the corresponding value for bulk gold/silver. This lowering of TCR value for the nanostructured film is indicative of a morphology similar to granular metals; wherein the apparent strain due to thermal expansion of the device and the positive TCR of metallic islands is offset by the negative TCR associated with thermally activated electron transport across the junctions [19]. The lower TCR value is advantageous for minimizing thermal drift during strain gauge operation.

C. Dynamic Response

Device response to dynamic strain inputs demonstrates a robust and repeatable response to both variations in amplitude of strain [see Fig. 5(a)] and variations in the frequency of applied strain [see Fig. 5(b)]. Furthermore, the device shows a durable response even after 500 bending cycles [see Fig. 5(c)–(e)]. The repeatability of these measurements is estimated to be 0.25%, based on the dynamic response. The excellent working range and dynamic response of the strain sensor demonstrated in this study render these suitable for applications such as structural monitoring [20], touch sensing [21], etc.

D. Human Motion Detection

To demonstrate the utility of the nanoparticle film for human motion detection, a stretchable substrate–a latex surgical glove–was

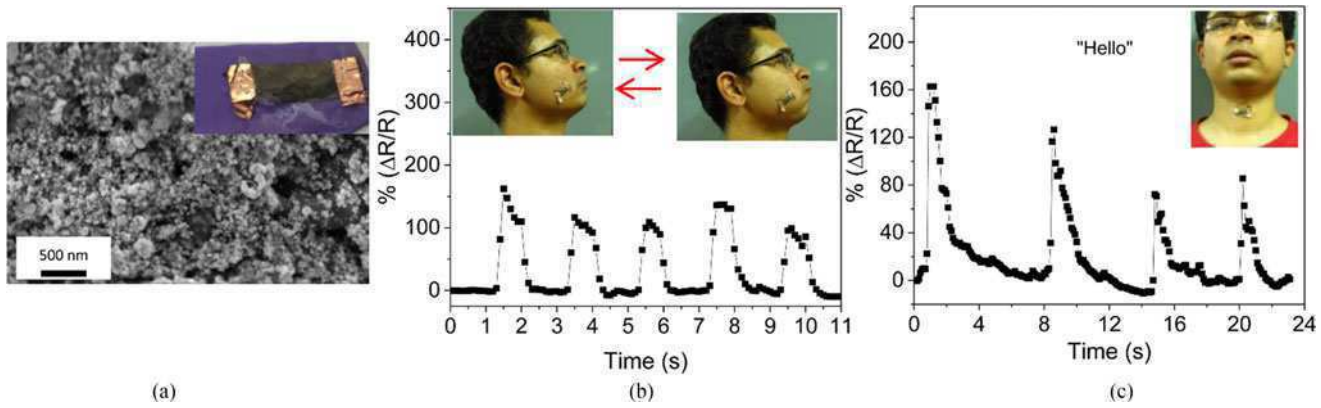

Fig. 6. (a) Representative FESEM image of gold coated silver nanoparticles on latex substrate. (Inset) Image of gold coated silver nanoparticles coated over a latex substrate with copper tape at both ends for electrical contact. Human motion detection demonstration of (b) cheek bulge motion and (c) phonetic recognition while uttering "Hello."

employed. A latex glove was cut through to create a flat surface and was coated with polyelectrolyte film followed by exposure to 1.5 M NaCl. Silver nitrate solution (0.5 M) was drop-cast to generate silver chloride film *in situ*. This film was then developed and toned to produce conductive nanoparticle film. Electrical contacts were established using silver ink and copper tape. Fig. 6(a) shows the image of the latex substrate along with FESEM image of the nanoparticle film. "Cheek-bulge" and phonetic detection experiments were accomplished by attaching the sensor onto skin with double-sided tape [see Fig. 6(b) and (c)].

IV. CONCLUSION

A low-cost, room-temperature process for *in-situ* fabrication of nanostructured metallic thin films on PET substrates has been demonstrated. The gold-toned silver nanoparticle films are highly sensitive to applied strain with a gauge factor of 25 that is comparable to earlier reports on metallic nanostructures fabricated using colloidal formulations. The fabricated devices have a low base-resistance as well as a small temperature coefficient of resistance, comparable to those of commercial strain gauges that are fabricated using lithography and etching. The printed strain gauges also exhibit an excellent dynamic response, rendering these suited for applications requiring flexible strain sensors on plastic substrates. Furthermore, the process is adaptable to stretchable substrates for human motion detection.

ACKNOWLEDGMENT

This work was supported in part by the Department of Science and Technology, Science and Engineering Research Board, Government of India, in part by the centre for infrastructure, Sustainable Transportation and Urban Planning, Indian Institute of Science (IISc), and in part Sustainable Transportation and Urban Planning, IISc, and in part by the Space Technology Cell, IISc.

The authors would like to thank the Centre for Nanoscience and Engineering and the Department of Mechanical Engineering, IISc, for access to instrumentation.

REFERENCES

[1] K. Hoffmann, *An Introduction to Measurements Using Strain Gages*. Darmstadt, Germany: Hottinger Baldwin Messtechnik, 1989.

[2] M. Gao, L. Li, and Y. Song, "Inkjet printing wearable electronic devices," *J. Mater. Chem. C*, vol. 5, no. 12, pp. 2971–2993, 2017, doi: 10.1039/C7TC00038C.

[3] M. Segev-Bar and H. Haick, "Flexible sensors based on nanoparticles," *ACS Nano*, vol. 7, no. 10, pp. 8366–8378, 2013, doi: 10.1021/nn402728g.

[4] B. Ando and S. Baglio, "All-inkjet printed strain sensors," *IEEE Sensors J.*, vol. 13, no. 12, pp. 4874–4879, Dec. 2013, doi: 10.1109/JSEN.2013.2276271.

[5] M. Bona, M. Serpelloni, E. Sardini, C. O. Lombardo, and B. Andò, "Telemetric technique for wireless strain measurement from an inkjet-printed resistive sensor," *IEEE Trans. Instrum. Meas.*, vol. 66, no. 4, pp. 583–591, Apr. 2017, doi: 10.1109/TIM.2016.2607958.

[6] V. Correia, C. Caparros, C. Casellas, L. Francesch, J. G. Rocha, and S. Lanceros-Mendez, "Development of inkjet printed strain sensors," *Smart Mater. Struct.*, vol. 22, no. 10, 2013, Art. no. 105028, doi: 10.1088/0964-1726/22/10/105028.

[7] Y. Wang, N. Li, D. Li, S. Yu, and C. Wang, "A bio-inspired method to inkjet-printing copper pattern on polyimide substrate," *Mater. Lett.*, vol. 140, pp. 127–130, 2015, doi: 10.1016/j.matlet.2014.11.006.

[8] R.-Z. Li, A. Hu, T. Zhang, and K. D. Oakes, "Direct writing on paper of foldable capacitive touch pads with silver nanowire inks," *ACS Appl. Mater. Interfaces*, vol. 6, no. 23, pp. 21721–21729, 2014, doi: 10.1021/am506987w.

[9] Y. Lee, W.-Y. Jin, K. Y. Cho, J.-W. Kang, and J. Kim, "Thermal pressing of a metal-grid transparent electrode into a plastic substrate for flexible electronic devices," *J. Mater. Chem. C*, vol. 4, no. 32, pp. 7577–7583, 2016, doi: 10.1039/C6TC01234E.

[10] Q. Huang, W. Shen, Q. Xu, R. Tan, and W. Song, "Room-temperature sintering of conductive Ag films on paper," *Mater. Lett.*, vol. 123, pp. 124–127, 2014, doi: 10.1016/j.matlet.2014.02.101.

[11] B. Wang, D. Hu, J. Nie, and X. Zhu, "Large-scale flexible conductive copper-silver pattern based on direct photo-patterning via volume additive process on demand," *Mater. Lett.*, vol. 188, pp. 296–299, 2017, doi: 10.1016/j.matlet.2016.10.107.

[12] S. K. Parmar and V. Santhanam, "In situ formation of silver nanowire networks on paper," *Current Sci.*, vol. 107, no. 2, pp. 262–269, 2014.

[13] K. Cheng *et al.*, "Ink-jet printing, self-assembled polyelectrolytes, and electroless plating: Low cost fabrication of circuits on a flexible substrate at room temperature," *Macromol. Rapid Commun.*, vol. 26, no. 4, pp. 247–264, 2005, doi: 10.1002/marc.200400462.

[14] P. Joshi and V. Santhanam, "Paper-based SERS active substrates on demand," *RSC Adv.*, vol. 6, no. 72, pp. 68545–68552, 2016, doi: 10.1039/C6RA07280A.

[15] S. Anchell, *The Darkroom Cookbook*, 3rd ed. Burlington, NJ, USA: Taylor and Francis, 2008, doi: 10.1016/B978-0-240-81055-3.50017-7.

[16] R. A. McAloney, M. Sinyor, V. Dudnik, and M. Cynthia Goh, "Atomic force microscopy studies of salt effects on polyelectrolyte multilayer film morphology," *Langmuir*, vol. 17, no. 21, pp. 6655–6663, 2001, doi: 10.1021/la010136q.

[17] L. Meng, S. M. Mahpeykar, Q. Xiong, B. Ahvazi, and X. Wang, "Strain sensors on water-soluble cellulose nanofibril paper by polydimethylsiloxane (PDMS) stencil lithography," *RSC Adv.*, vol. 6, pp. 85427–85433, 2016, doi: 10.1039/C6RA10069D.

[18] J. Herrmann *et al.*, "Nanoparticle films as sensitive strain gauges," *Appl. Phys. Lett.*, vol. 91, no. 18, 2007, Art. no. 183105, doi: 10.1063/1.2805026.

[19] L. Yi *et al.*, "Ultrasensitive strain gauge with tunable temperature coefficient of resistivity," *Nano Res.*, vol. 9, no. 5, pp. 1346–1357, 2016, doi: 10.1007/s12274-016-1030-0.

[20] J. Sebastian *et al.*, "Health monitoring of structural composites with embedded carbon nanotube coated glass fiber sensors," *Carbon*, vol. 66, pp. 191–200, 2014, doi: 10.1016/j.carbon.2013.08.058.

[21] M. Segev-Bar, A. Landman, M. Nir-Shapira, G. Shuster, and H. Haick, "Tunable touch sensor and combined sensing platform: Toward nanoparticle-based electronic skin," *ACS Appl. Mater. Interfaces*, vol. 5, no. 12, pp. 5531–5541, 2013, doi: 10.1021/am400757q.